LUBRICATION AND WEAR AT METAL/HDPE CONTACTS

A Thesis
Submitted to the Graduate Faculty
of the
North Dakota State University
of Agriculture And Applied Science

By

Aydar Akchurin

In Partial Fulfillment of Requirements
for the Degree of
MASTER OF SCIENCE

Major Department:
Mechanical Engineering

October 2012

Fargo, North Dakota

North Dakota State University
Graduate School

Title

Lubrication and Wear at

Metal/HDPE Contacts

By

Aydar   Akchurin

The Supervisory Committee certifies that this *disquisition* complies with North Dakota State University's regulations and meets the accepted standards for the degree of

MASTER OF SCIENCE

SUPERVISORY COMMITTEE:

Dr. Iskander Akhatov

Chair

Dr. Annie Tangpong

Dr. Andriy Voronov

Dr. Yechun Wang

Approved:

11/8/2012	Dr. Alan Kallmeyer
Date	Department Chair

ABSTRACT

In the thesis lubrication and wear at metal/HDPE contacts was addressed. In particular this type of contact occurs in artificial joint replacements. Wear of HDPE was recognized as a major factor limiting device performance.

In the thesis, fully implicit fully coupled numerical approach was developed to simulate lubrication and wear. Approach allows solving stationary and transient problems for rough surfaces in a wide range of parameters. Wear coefficients were estimated from experimental data.

Wear particles formed in wear process were investigated. Particles were found to be approximately 100 nm in diameter and spherical in shape. Considering theoretical solutions, it was concluded that debris may play a role of third-body abrasive wear particles.

In the summary section, some discussion was provided on the topic of theoretical modeling of friction and wear and recommendations for future research were formulated.

ACKNOWLEDGEMENTS

TABLE OF CONTENTS

LIST OF TABLES

LIST OF FIGURES

1. INTRODUCTION

1.1. Lubrication

It has been empirically recognized long time ago that dry contacts between sliding or rolling solid bodies produce higher friction forces than lubricated ones. At the same time such surfaces wear out considerably faster and correspondingly an operational life of a machine element or a whole machine is shortened drastically. These phenomena are closely related and play important role in our life.

Sometimes friction is a desirable force, like in a case of brakes operation, or Stone Age practice of firing by friction heat, but in other cases the influence of it must be reduced to a minimum. Humans developed different approaches to decrease friction, but one of the most powerful ways to accomplish the task is lubrication. Although lubrication is possible by means of gases, semifluid (greases) and even solid materials, most effective lubrication is provided by liquids. In such contacts liquids manage to penetrate between surfaces, build a separation fluid film, reduce friction, improve heat dissipation, carry most of the load and prevent excessive destruction.

It should be mentioned, that the parameters of our interest in lubrication theory are film thickness and pressure. Film thickness determines how well two surfaces are separated to avoid direct contact and pressure determines how strong the influence of the load on the bodies is.

Practically important devices with lubrication are met in many areas including aerospace, power generation, transportation, defense, manufacturing, computer technology and biomechanical engineering (Fuller 1984). Artificial joint replacement in biomechanical engineering is a particular example of such a device where two articulating surfaces are

separated by synovial fluid and pressed against each other by load. One of these surfaces usually is made from plastic material, for example, high density polyethylene (HDPE) (Charnley 1976).

1.2. Wear

Friction sometime is inevitable and necessary phenomena, but wear has always negative consequences, whether it happens with personal belongings or with public properties. Obviously, any wear process cost money. For example, wear of clothes, shoes, tires, doors, and stairs makes us to spend money on replacements and repairs. It was calculated by different sources that personal wear costs are about 25 – 250 dollars per year (in 1966) (K.C. 1996). In a scale of a nation, road wear, automotive and air jet engine wear, rail road and bridges, and many other sources of wear require constant investment in repair, replacement, related energy consumption costs, overall decreasing nation's productivity. Wear also affects biomedical applications, such as artificial joint replacements, causing significant operation life reduction of this device (Ingham E. 2005, Sargeant A. 2006). Thus, significant and continuous efforts have been provided to the field of wear research and wear reduction (Wood W.J. 2011, Wannasria S. 2009).

There is an increasing interest in the wear of plastic materials, such as polytetrafluoroethylene (PTFE), high density polyethylene (HDPE), ultra high molecular weight polyethylene (UHMWPE) in application to artificial joint replacements. These materials do not wear out completely, however, despite of favorable mechanical properties, materials produce considerable wear debris amount to initiate autoimmune response and bone loosening. As a consequence, revision surgery could be needed (Akchurin A. 2012).

Thus, increasing the wear resistance of artificial joint replacement materials is one of the primary goals of modern arthroplasty.

1.3. Thesis objective

As it was pointed out in the previous paragraphs, biomedical engineering devices, such as joint replacements, are worn out inducing health problems. Major cause of these problems is the wear of a plastic material and reduction of it could improve life quality of such patients. Therefore, the objective of this research was to develop a theoretical model which predicts wear of HDPE in lubricated conditions as a function of the operational parameters. Dependency of wear and friction on these parameters can help to optimize the design of such devices. Obviously, experiments were required to verify the model.

1.4. Overview

Chapter 2 of the thesis presents literature review on the topic of lubrication and wear with emphasis in lubrication models, as the major phenomenon of the process. Chapter 3 is devoted to the theoretical development of a general lubrication model and governing equations. In a following Chapter 4, major analytical solutions obtained for several cases. In Chapter 5, numerical solution approach is described and obtained solutions are discussed. Experimental measurements of friction coefficient and wear mass loss are presented in Chapter 6. Comparison of theoretical results with experiments is given in Chapter 7. Wear particle measurements and possible relation with theory are provided in Chapter 8. Some conclusions and suggestions are summarized in Chapter 9.

2. LITERATURE REVIEW

2.1. Artificial joint replacements

As it was mentioned above, the primary concern of the thesis is the lubrication in artificial joint replacements. The reason for this is the increasing demands in such kind of devices for patients with joint pain, as it is shown in Figure 1. Abbreviation TKA stands for total knee arthroplasty, whereas THA for total hip arthroplasty.
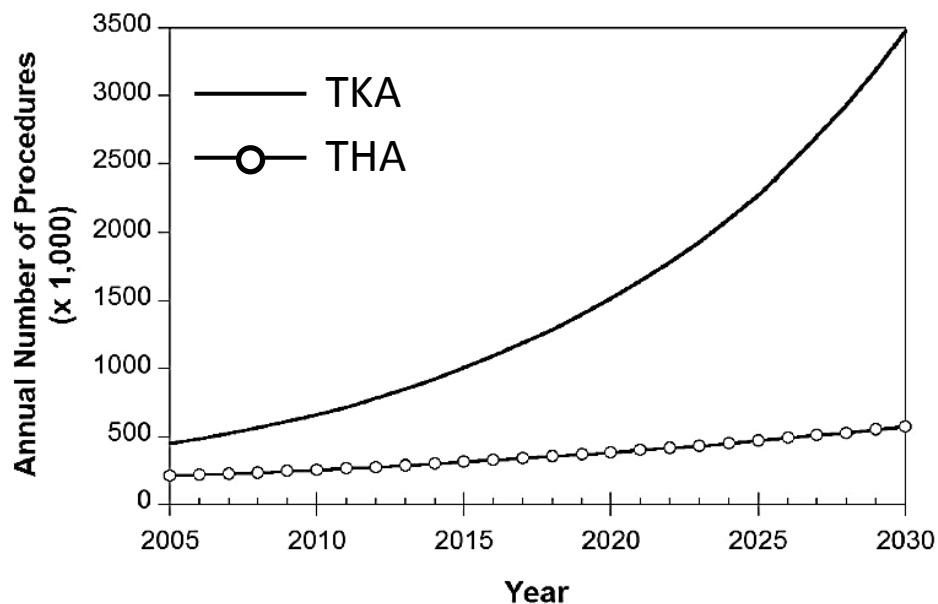
Figure 1. Projections of primary replacement surgeries (Kurtz S. 2007).

Under healthy conditions, natural joint works under lubricated condition with synovial liquid acting as a lubricant. The bearing surfaces are represented by human bones with surfaces covered by layers of articular cartilage. Interaction of this material and synovial fluid under normal conditions develops very low friction (the range for friction coefficient is in 0.005 to 0.04, (Kennedy F.E., Natural and Human Joints 2012)) and negligible wear during the lifetime of the human. From the point of view of tribological performance of the joint, synovial fluid is the major component. The main constituent of it

4

is water and it also contains long chain protein molecules, hyaluronic acid and phospholipids (Neville 2007). Synovial fluid shows strongly non-Newtonian properties with viscosity varying in the range from about 0.05 to 1.5 Pa s, depending on operational conditions, as well as individual features of the human (Kennedy F.E., Natural and Human Joints 2012). Operational conditions important to lubrication analysis in joints can be summarized in a Table 1, (Neville 2007).

Table 1. Operational conditions in joints.

Motion	Sliding/rolling
Lubrication regime	Hydrodynamic/Boundary lubrication
Speed	0.03-0.3 m/s
Contact pressure	Max 18 MPa
Temperature	25-40 °C

Brilliant performance of natural joints sometimes fails and people start to feel pain. In this case, replacement surgery is performed, and artificial joint replaces the natural one. Schematic of such device for THA is shown in Figure 2.

Acetabular Cup
Polyethylene Liner
Femoral Head
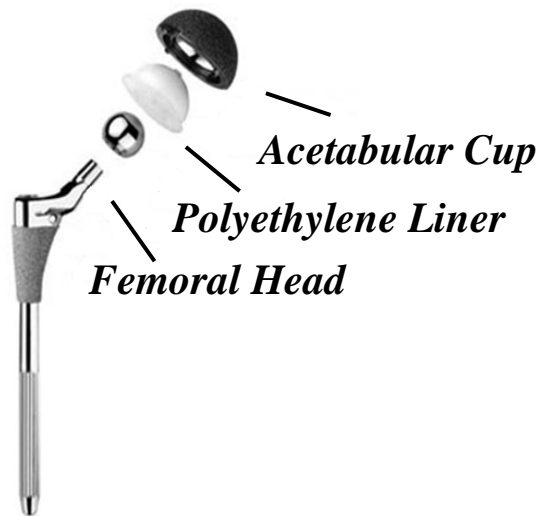
Figure 2. Schematic representation of artificial hip replacement.

In a shown case, femoral head and polyethylene liner are the bearing surfaces, and as in case with natural joints, they operate in synovial lubrication environment. First introduced by Charnley in 1962 (Kennedy F.E., Natural and Human Joints 2012), these devices showed low friction and wear performance and are able to relief patients from pain. However, sometimes they fail resulting revision, which is a risky and expensive surgery. At the same time, younger people need joint replacements demanding additional requirements to the performance and longevity of artificial joints. Projections of these revision surgeries are shown in Figure 3
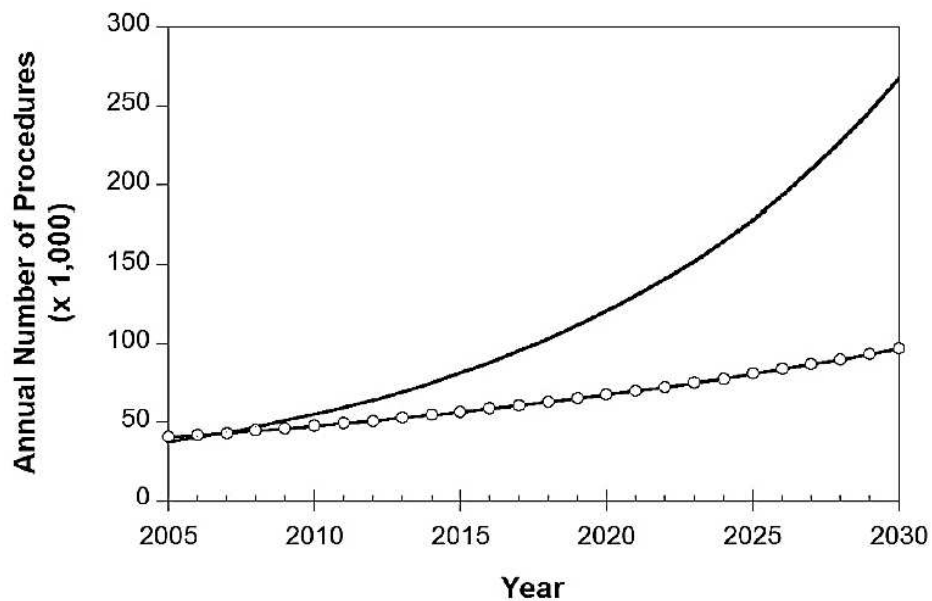
Figure 3. Projection of revision surgeries (Kurtz S. 2007).

It is already admitted by researchers that the major reason of joint failure is the wear of polyethylene liner (Atwood S. A. 2006). However, the primary failure is not due to mechanical wear through of the liner, but the wear-particle induced immune system reaction (osteolysis, resorption of living bone tissue), which leads to a joint loosening (A. 2012). Thus, increasing the wear resistance of artificial joint replacement materials is one of the primary goals of modern arthroplasty.

A number of researchers attempted to study the lubrication and wear in artificial joints theoretically as it was recently reviewed by Mattei et al (Mattei L. n.d.). Goenka (Goenka P 1980) was first to formulate transient Reynolds equation in spherical coordinates and solve it using finite element analysis. Using Newton-Raphson approach a simultaneous solution of elasto-hydrodynamic lubrication (EHL) problem for ball-in-socket geometry was obtained by Jalali-Vahid et al (Jalali-Vahid D 2003). A general methodology for steady state EHL analysis of hip implants was developed by Jagatia et al (Jagatia M. 2001). Newton-Raphson algorithms of Reynolds equation with finite element analysis to obtain elastic deformations were used for solution. Sparse fast Fourier transformation approach allowed Wang et al (Wang F.C. 2004) to solve EHL problem for realistic 3D loading and motion of walking conditions. However, in case when solution requires highly dense mesh, Newton-Raphson approach becomes inefficient as a full matrix linear system must be solved, which is much more expensive in terms of calculation resources (Gao L. M. 2007). For this reason, multi-grid techniques introduced by Lubrecht and further improved by Venner (Venner C.H. 2000) are widely employed in EHL analysis of artificial joint replacements. As it will be discussed in more details later in the thesis, recently developed be Evans et al (Evans H. P. 2000) differential deflection approach allows overcoming mentioned drawback and obtaining EHL solution in an efficient manner using Newton-Raphson solver.

In wear modeling of artificial joint replacements, situation is even more complicated, due to complex nature of the considered phenomena itself. Most of the studies neglect the lubrication (Mattei L. n.d.) and consider Archard's wear law (Archard 1953) to estimate wear factor, or wear coefficient from experimental measurements (Kima N. H.

2005, Mukrasa S. 2009, Benabdallah H. 2006). Using this approach, Fisher et al (Fisher J. 1994) explored dependency of wear factor on roughness and sliding speed and obtained empirical relationship between wear factor and roughness of the tough counter face in case of bovine serum lubricated conditions. Wang (Wang 2001) developed a different wear law for UHMWPE in multi-directional sliding in lubricated contact. However, the law was not coupled with EHL theory, which again means that the influence of lubrication was neglected. Kennedy et al (Kennedy F.E., Lubrication and Wear of Artificial Knee Joint Materials in a Rolling/Sliding Tribotester 2007) explored wear of UHMWPE in oscillating contacts and using Archard's law found that the wear factor along the wear track in case of lubricated contact varies in different locations. EHL theory was employed to explain this result, however, estimation of wear factor was solely based on the simplified dry Hertz theory solution, which may fail in the lubricated contacts.

As the normal function of either artificial or natural joints is highly dependent on the synovial liquid lubrication, assumption of dry contact may not be fulfilled. Thus, for a proper wear analysis, lubrication theory cannot be neglected. Zhu et al (M. A. Zhu D. 2007) built a sequential numerical algorithm to solve coupled lubricant flow and wear of material. As it will be discussed later in the section devoted to numerical approach, there are some disadvantages of sequential algorithm, mainly related to the low convergence speed of such schemes. In case of modeling a transient problem for rough surfaces, high number of EHL solutions coupled with wear theory must be built. For example, for the modeling of one wear cycle of a pin-on-disk machine, it is necessary to solve the problem at least 300 times, depending on the time step discretization. Thus, low convergence speed algorithms cannot be efficiently applied to the wear simulation. For this reason, in the

thesis, a fully implicit or simultaneous approach of coupling Archard's wear law with EHL theory was developed.

2.2. Lubrication theory

History of lubrication theory goes more than a century back to 1886 when O. Reynolds published famous equation of thin fluid film flow in the narrow gap between two solids (Reynolds 1886). This equation carries his name and forms a foundation of the lubrication theory. First analytical solutions for pressure distribution in case of parallel and converging plane surfaces with fixed separation film thicknesses were obtained by Reynolds himself.

Further, in 1916 Martin (Dowson D., Elasto-Hydrodynamic Lubrication. SI Edition. 1977) obtained a closed form solution for a minimum film thickness and pressure for a cylinder and plane geometry under assumptions of rigid surfaces and isoviscous lubricants. But as it was shown experimentally later, this solution did not match with film thickness measurements in case of high loads. Comparison of Martin's rigid body solution with experimental measurements can be seen on Figure 4.

Derivation of several analytical solutions including this one will be shown further in the thesis and it will be seen that pressure distribution is fully determined by minimum film thickness and therefore is of most importance in theoretical analysis.

Divergence of experimental and theoretical results by Martin for high loads leaded researchers to conclusion that elastic distortion and pressure-viscosity dependence play a significant role in lubrication. In 1949, Grubin (Grubin A.N. 1949) obtained a solution for so called elasto-hydrodynamic lubrication (EHL) line contact problem with certain simplifications, where he combined both elastic deformation and lubricant hydrodynamic

flow. Although his solution did not satisfy both elastic and hydrodynamic equations of EHL, his analysis was recognized as particularly useful. It also included variance of viscosity with pressure. At the same time, Grubin was able to predict formation of pressure spike at the outlet region – remarkable feature of EHL solutions.
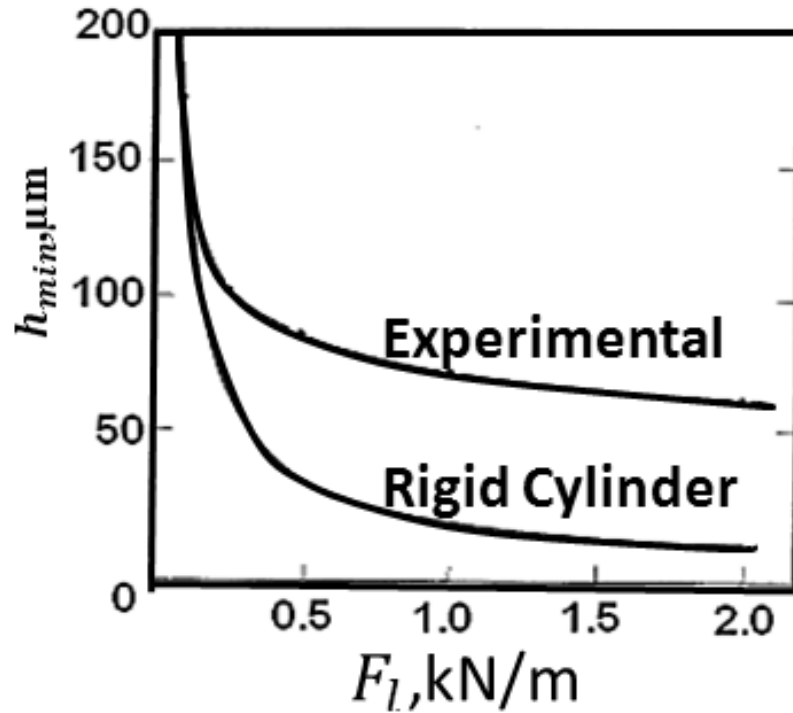
Figure 4. Variation of film thickness with load, (Dowson D., Elasto-Hydrodynamic Lubrication. SI Edition. 1977).

Petrushevich (Petrusevich 1951) was actually first to obtain predicted by Grubin pressure spike in his numerical analysis of the EHL line contact problem. For this reason, the spike sometimes is referred to as "Petrushevich" spike. Obtained in 1951, his solution was first solution of combined elastic distortion, fluid flow and pressure-viscosity dependency equations. It should be emphasized, that the occurrence of the pressure spike is closely related to the variance of viscosity with pressure along with elastic properties of

materials and relative speed. In the thesis, it was noticed that pressure spike does not occur, if only constant pressure is considered.

Remarkable analytical solution of a point contact problem was derived by a famous Russian scientist P.L. Kapitsa (Cameron 1976) in assumptions of rigid substrates, isoviscous fluid and half-Sommerfeld boundary conditions. Under these conditions, he obtained a closed form relation of minimum film thickness on load and other parameters of the problem.

By that moment, newly introduced computer technologies became available. Further development of the solution approaches was closely related to the growth of computer capabilities and evolution of numerical methods.

In 1959 Dowson and Higginson (Dowson D., A Numerical Solution to the Elastohydrodynamic Problem 1959) computed series of numerical solutions of EHL line contact problem for a range and obtained a regression formula for a minimum film thickness, which is still being widely used. They also introduced three non-dimensional groups of parameters, namely "load", "speed" and "materials" parameters. Equation is given by:

$$\frac{h_0}{R} = 2.65 \bar{U}^{0.3} \bar{G}^{0.54} \bar{W}_L^{-0.13} \qquad (\,1\,)$$

where $\bar{W}_L = F_L/E'R$ is the load parameter, $\bar{G} = \alpha E'$ is the materials parameter and $\bar{U} = U\mu_0/E'R$ is the speed parameter.

Several approaches were introduced to solve the system of EHL equations. Direct methods are used to obtain the pressure distribution for a known fluid film thickness and inverse methods vice versa: for a fixed pressure distribution, fluid film thickness is calculated (Gohar 1988).

Multigrid approach introduced by Lubrecht (Lugt P.M. 2011) and further improved by Venner (Venner C.H. 2000) significantly increased efficiency of numerical methods and allowed researchers analyze more complex problems. Recently, a fully implicit approach along with Newton's method was reexamined in a light of development of differential deflection approach (Evans H. P. 2000). Advanced computational methods combined with sophisticated hardware nowadays allow tribologists to explore transient problems (Wijnant 1998), incorporate plastic effects (Ning Ren 2010), surface roughness (H. Y.-Z. Zhu D. 2001), study thermal problems (Hasim Khan 2009), mixed EHL (Hu Y.Z. Wang H. 2001) and wear processes (M. A. Zhu D. 2007). Recently, CFD (Hartinger 2007) and molecular dynamic simulations (Spikes 2006) were employed in EHL problems.

3. FORMULATION AND GOVERNING EQUATIONS

As long the lubrication in joints is analyzed, some theoretical and experimental models must be considered. In general, a complex three-dimensional motion and three-dimensional dynamic loading makes is difficult to simulate and investigate behavior of natural and artificial joints. Thus, some simplifications are employed, namely, one-dimensional loading and one-directional motion. It allows then using a pin-on-disk tribometer for experimental measurements of wear and friction. The simplified problem formulation is shown in the Figure 5.
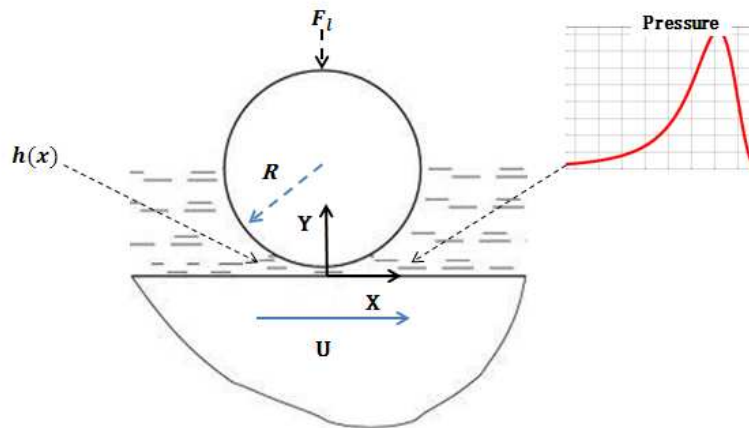
Figure 5. Schematic representation of the problem.

Instead of 3-D problem, a 2-D simplified approach is employed. A cylinder with radius R with some length in Z direction is considered and it is assumed that nothing changes in that direction. There is some lubricant between the steel cylinder and the HDPE substrate with certain viscosity, and thickness of this lubricant layer changes with

coordinate X. Coordinate system is fixed and related to the steel cylinder. The substrate moves with constant velocity U, and the steel cylinder is stationary. When some load is applied through the cylinder, a certain pressure is developed in the lubricant and equilibrate applied load. As long as the elastic modulus of steel is two orders of magnitude higher than of HDPE, the cylinder is considered to be rigid, and only substrate is allowed to deform elastically.

Unknowns here are the pressure developed in lubricant and, actually, separation distance between two bodies, which is lubricant film thickness. Knowing these values, one can estimate friction, and through some laws estimate wear. And it is important to know, how these variables depend on the given parameters, like load, viscosity, speed and any other related values.

In general, EHL model involves two groups of equations (Ai 1993). First group consists of:

1) Reynolds equation

2) Film thickness equation

3) Load balance equation

Second group involves empirical relationships:

1) Viscosity-pressure relation

2) Density-pressure relation

Further, this system of equations can be changed in order to account non-Newtonian behavior, temperature, plastic deformations, time dependent geometry (roughness, wear) and other effects.

3.1. Reynolds equation

Reynolds equation is the result of classical Reynolds theory and is employed in a wide range of thin film flow problems. The principles of the theory are derived from the observation that the lubricant can be treated as isoviscous and laminar and the fluid film is of negligible curvature. Reynolds equation can be derived from the Navier-Stokes equations and the equation of continuity under assumptions of:

1) constant viscosity, Newtonian lubricant

2) thin film geometry

3) negligible inertia

4) negligible body force

Under these assumptions one can obtain following equation (Szeri 2005):

$$\frac{\partial}{\partial x}\left(\frac{\rho h^3}{12\mu}\frac{\partial p}{\partial x}\right) + \frac{\partial}{\partial y}\left(\frac{\rho h^3}{12\mu}\frac{\partial p}{\partial z}\right) - \frac{\partial(u_m \rho h)}{\partial x} - \frac{\partial(\rho h)}{\partial t} = 0 \qquad (\,2\,)$$

where p is the pressure, h is the film thickness or gap height, t the time, ρ the density, μ the viscosity of lubricant and $u_m = \frac{U_1 + U_2}{2}$ represents the mean velocity of the surfaces. First two terms in equation represent Poiseuille pressure induced flow, the third one is referred to as Couette term describing the flow induced by mean velocity and the last is known as a squeeze term. A sketch with coordinate axes and velocities is shown in a Figure 4.
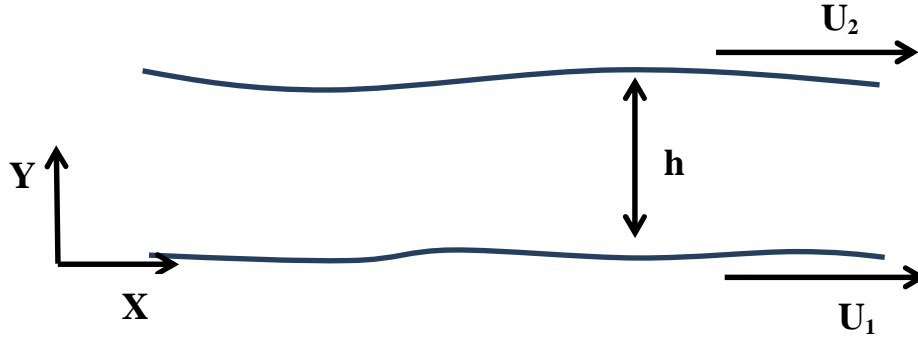
Figure 6. Surfaces in a relative motion.

Equation (3) is called Reynolds equation and is, in fact, three- dimensional. In a following analysis, a simplified two-dimensional version is used:

$$\frac{\partial}{\partial x}\left(\frac{\rho h^3}{12\mu}\frac{\partial p}{\partial x}\right) - \frac{\partial(u_m\rho h)}{\partial x} - \frac{\partial(\rho h)}{\partial t} = 0 \qquad (3)$$

3.2. Elastic deflection equation

As long as EHL problems require evaluation of elastic deflection, expression for relating pressure and deflection is needed. Detailed derivation of it is given in (Dowson D., Elasto-Hydrodynamic Lubrication. SI Edition. 1977), (Johnson 2003), (Timoshenko S. 1951). Equation is derived for a semi-infinite perfectly elastic body, shown in Figure 7. It is supposed that in directions z, y bodies are infinite and in the study only vertical deflections are of interest.
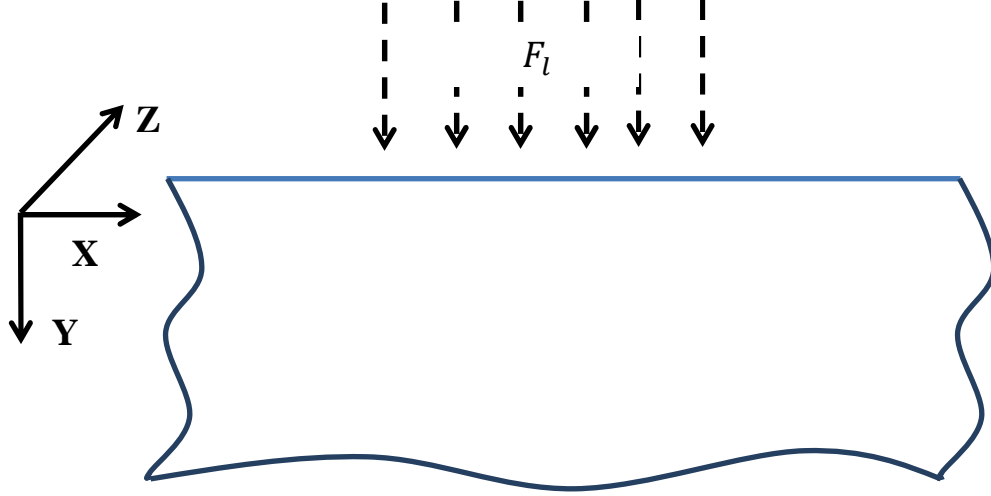
Figure 7. Semi-infinite elastic half-space.

In the examined case, consideration of semi-infinite elastic half-space is justified, as the elastic deflection is orders of magnitudes smaller than actual size of the analyzed substrate. In this case, analytical solution of equations of elasticity theory gives following:

$$h_e(x) = -\frac{4}{\pi E'}\int_{x_a}^{x_c} p(x')\ln(x - x')\,dx' + C \qquad (4)$$

where $h_e(x)$ is elastic deflection, $p(x')$ - pressure, $1/E' = (1 - v^2)/E$ – reduced Young's modulus, E – Young's modulus, v – Poisson's ratio and C is constant. This constant is taken in the way, to make the deflection equal zero somewhere significantly far from the contact. For example, if at a point x_a deflection is zero, then constant is equal to:

$$C = \frac{4}{\pi E'}\int_{x_a}^{x_c} p(x')\ln(x_a - x')\,dx' \qquad (5)$$

In case of two elastically deformable bodies, reduced elastic modulus can be calculated as an arithmetic average:

$$\frac{1}{E'} = \frac{1}{2}\left(\frac{1}{E_1'} + \frac{1}{E_2'}\right) \qquad (6)$$

In the thesis, a metal/HDPE contact is considered and consequently, metal ball can be considered as a rigid body compared to the HDPE substrate.

It is clear from equation (4) that deflection at each point depends on pressure distribution all over the substrate, which makes the final system of equations differential-integral and complicates numerical solution.

3.3. Film thickness equation

In the examined two dimensional case, instead of a three dimensional ball, a simple geometry of an infinite cylinder is introduced as it is shown in a Figure 8. Hence, the problem becomes two dimensional. First, consider only the ball and assume zero point coincides with its vicinity.
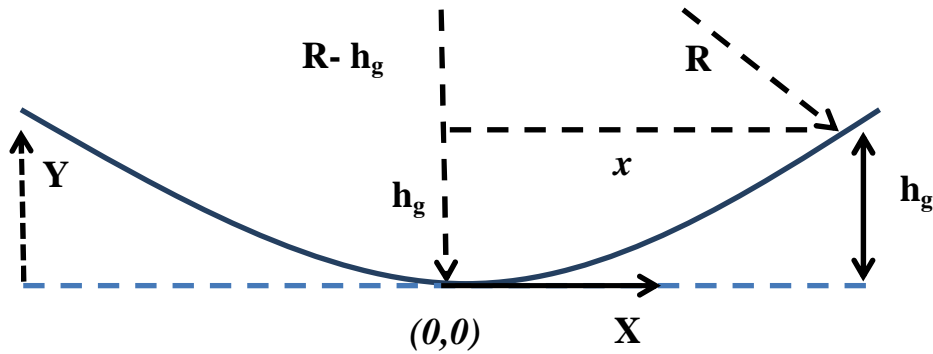
Figure 8. Geometrical component of film thickness.

Near the vicinity at point $x = 0$, thickness h_g can be represented as a function of a current ordinate x and approximated by neglecting all terms of Taylor's expansion with exponents higher than two:

$$h_g(x) = R\left(1 - \left(1 - \left(\frac{x}{R}\right)^2\right)^{1/2}\right)$$

Taylor's expansion near zero:

$$\left(1 - \left(1 - \left(\frac{x}{R}\right)^2\right)^{1/2}\right) \approx \frac{x^2}{2R^2}$$

and hence,

$$h_g(x) = \frac{x^2}{2R} \tag{7}$$

Further, we can introduce a substrate on a distance h_0 from the cylinder as it is shown in the Figure 4.
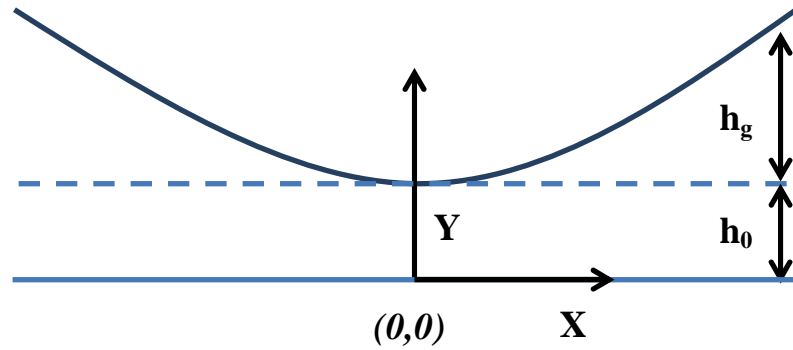
Figure 9. Cylinder and substrate.

Then the distance between the cylinder and the substrate could be written as follows:

$$h(x) = h_0 + h_g(x) \tag{8}$$

This gap is considered to be filled by a lubricant and hence, $h(x)$ is a lubricant thickness, or film thickness. Further, if there is an applied load, some pressure distribution is going to arise and the substrate is going to deflect according to equation (4). This deformation $h_e(x)$ will increase the distance between surfaces and hence equation (8) is re-written:

$$h(x) = h_0 + h_g(x) + h_e(x) \tag{9}$$

19

It should be emphasized, that parameter h_0 in equation (9) cannot be treated as in (8) as a minimum distance between two surfaces. Now h_0 represents only a distance between line $y = 0$ and the cylinder vicinity necessary to equilibrate applied load. This parameter is unknown and has to be calculated using force balance equation.
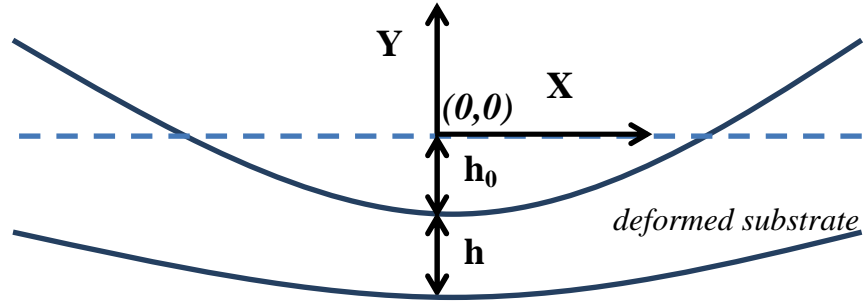
Figure 10. Geometrical meaning of h_0.

In case shown in the Figure 10, h_0 has a negative value according to equation (9) at $x = 0$. In general, it can be a positive number, if the cylinder does not cross the line $y = 0$.

Equation (9) is not a complete expression for the film thickness, as there are not included surface roughness and wear, which directly affect separation thickness. It will be done later in the thesis.

Pressure distribution over a fluid film is highly dependent on the film thickness. For EHL problems, elastic deformation of the contracting solids is important and influences the gap formation. Thus, final gap between surfaces consists of actual geometry and elastic terms. In the other hand, elastic effect is determined by pressure distribution. Hence, Reynolds equation and gap thickness formula in EHL problems are strongly coupled.

3.4. Wear law

Wear simulation allows studying the process precisely, finding parameters of most importance, substituting experiments and, actually, getting some important numbers. At the same time, wear itself is a very complicated process, which includes physical and chemical transformations. This fact gives rise to a high number of proposed wear models. According to the literature surveys (Meng H.C. 1995), the model proposed by Archard (Archard 1953) is most frequently used:

$$V_w = k_w F s \tag{10}$$

where V_w is wear volume, k_w is wear coefficient, F is the load and s is a sliding distance.

Now, if both parts of equation (10) are divided by the area of contact, equation takes form:

$$h_w = k_w p s \tag{11}$$

where h_w is a depth of wear and p is pressure.

In the other hand, when the transient problem is considered, h_w depends on time and distance can be represented in an incremental form:

$$dh_w = k_w p u \, dt \tag{12}$$

and hence,

$$\frac{dh_w}{dt} = k_w p u \tag{13}$$

Consider an arbitrary pressure distribution as shown in the Figure 11.
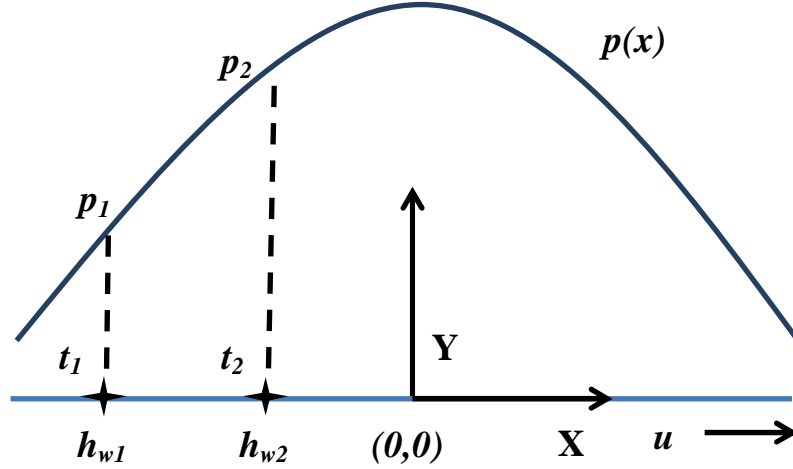
Figure 11. Motion of the worn point on a lower surface.

The coordinate system is fixed and zero point is on the lower surface under the vicinity of the cylinder. Consider a point of the surface at moment t_1 which experiences pressure p_1 and wear depth due to p_1 is h_{w1}. Suppose the coordinate of it is x. It is necessary to follow this point to find it at moment t_2 under pressure p_2 at coordinate $x + u(t_2 - t_1)$ with wear depth due to p_2 is h_{w2}. Total wear depth of this point then is $h = h_{w1} + h_{w2}$. Hence, following expression for wear in fixed coordinate system can be written:

$$h_w(x + ut, t) = k_w u \int_0^t p(x + ut', t') dt' \qquad (14)$$

Thus, every time step, there will be a wear generated by pressure. This wear will increase distance between two surfaces and hence must be incorporated into film thickness equation as a positive term:

$$h(x) = h_0 + h_g(x) + h_e(x) + h_w(x) \qquad (15)$$

The fact that the film thickness influences pressure distribution means that wear also influences pressure, and it plays a pressure dissipation role.

3.5. Surface roughness

It is well known that any surface is not ideally flat as it was supposed in previous sections. Some irregularities of the surfaces are always present and actually, in case of highly loaded contacts can play significant role, as the height of these asperities becomes comparable with minimum film thickness. This leads to the local rise of pressures and corresponding increase in wear, friction, temperature and other effects. Thus, proper treatment of surface roughness should be provided. Obviously, minimum film thickness must ensure a full separation of two bodies by a lubricant. To achieve it, film thickness must be larger than a sum of asperities height of the two bodies. Thus, asperity heights determine optimum parameters to achieve a full separation.

In general, asperities decrease the distance between the bodies, thus, equation for film thickness is re-written with account of asperities height as:

$$h(x) = h_0 + h_g(x) + h_e(x) + h_w(x) - s(x) \tag{16}$$

where $s(x)$ is an a sum of asperity heights of two bodies at point x. It is possible to introduce roughness from direct measurements of the surface, for example, by atomic force microscopy, or for simplicity, through mathematical expression. We can consider a following function:

$$s(x) = A_m \sin(\lambda x) \tag{17}$$

where A_m is an amplitude of the asperities, λ is a wave length.

Using this relation it is possible to analyze influence of amplitudes and roughness wave length on local film thicknesses and pressures. Moreover, if there are actual measurements of surface roughness, it is possible to fit them using equation (17) at some extent and get averaged values.

3.6. Load equation

Equilibrium of forces is reached when the hydrodynamic pressure obtained from Reynolds equation is balanced by applied load F_l. For the line contact problem the force balance is written as:

$$F_l = \int_{x_a}^{x_c} p(x')dx' \qquad (18)$$

where F_l is a load per unit length.

Hydrodynamic pressure in lubricant film acting on the upper surface, actually initiates two components of forces, in vertical and horizontal directions. But the horizontal component of it is very small, as the radius of curvature is very large compared to the contact length. Thus, it can be neglected.

3.7. Lubricant properties

Pressure dependent parameters of the fluid, such as viscosity and density are related with pressure through empirical equations. As the nature of these relations is empirical, various formulas are available for both properties (Venner C.H. 2000).

Probably, one of the most used equations is known as Barus equation:

$$\mu(p) = \mu_0 \exp\left(\alpha(p - p_0)\right) \qquad (19)$$

where μ_0 is the viscosity under atmospheric pressure and α is the pressure-viscosity coefficient.

The density can be assumed constant or again several experimental results can be employed. Dowson and Higginson (Dowson D., Elasto-Hydrodynamic Lubrication. SI Edition. 1977) relation is given by:

$$\rho(p) = \rho_0 \frac{5.9 \cdot 10^8 + 1.34p}{5.9 \cdot 10^8 + p} \qquad (\,20\,)$$

where ρ_0 is the atmospheric density and pressure unit is given in Pa.

Defined set of equations with corresponding boundary conditions forms a full stationary EHL problem. Boundary conditions will be discussed in the numerical scheme section. Developed code contains ability of pressure dependent density feature, however, pressures developed for metal/HDPE contacts are too small to influence the pressure distribution, and thus, in calculations were not considered.

3.8. Boundary conditions

Reynolds equation as the second order differential equation requires two boundary conditions to be stated. In one hand side, it is clear that far to the left from the contact in considered two dimensional cases pressure must be equal to atmospheric pressure. Thus, one of the boundary conditions for the problem is written as:

$$p(x_a) = p_0 \qquad (\,21\,)$$

With the same consideration, pressure on the right boundary is supposed to be equal to atmospheric pressure:

$$p(x_c) = p_0 \qquad (\,22\,)$$

Numerical solution of Reynolds equation with conditions stated boundary conditions is shown on the Figure 12 and is referred to as *Full Sommerfeld Solution*. Pressure distribution is asymmetric and contains negative values. This behavior is not physically justified, because the fluid cannot sustain pressures below its cavitation pressure (Floberg 1961).
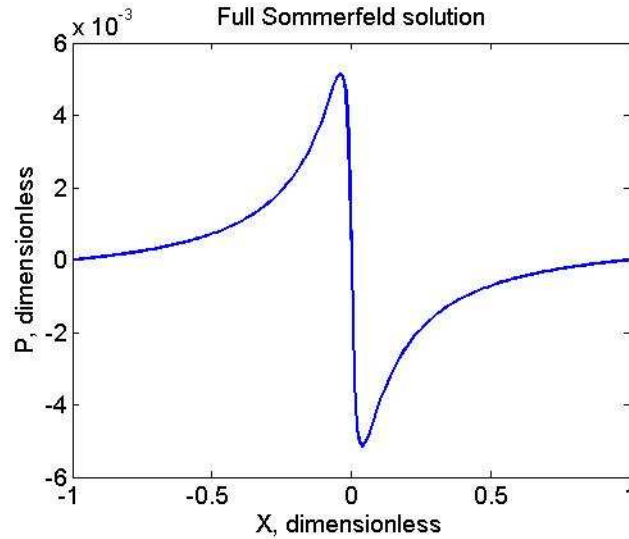
Figure 12. Full Sommerfeld numerical solution.

If the pressure goes below vapor, lubricant starts boiling. This condition is believed to happen rarely in lubrication problems (Dowson D., Elasto-Hydrodynamic Lubrication. SI Edition. 1977). In the other hand, if pressure falls below atmospheric, dissolved gases are liberated, forming bubbles and these bubbles maintain pressure near to saturation point. For examined case, saturation pressure is close to atmospheric, as the lubricant is opened to atmosphere. Such condition is called cavitation and needs to be implemented into numerical scheme. Complementarity arises when Reynolds equation is solved along with cavitation condition: full solution is subdivided into two areas. Within the one of them Reynolds equation solution is taken and within other one pressure is set to zero. The border between subdomains is unknown and there are several ways to find it.

The simplest way is known as *Half Sommerfeld Solution* and is used to estimate real pressure profile and load capacity. This approach simply set hydrodynamic pressure obtained by Reynolds equation to zero wherever it is negative. It is stated by Venner (Venner C.H. 2000) that half Sommerfeld solution results relatively small errors in determination of load capacity.

It was first noticed by Reynolds that proper boundary conditions are needed. To locate the cavitation point, one more equation is needed. Following equation is referred to as Reynolds, or Swift-Stieber boundary condition:

$$\frac{\partial p}{\partial x}\bigg|_{x_c} = 0 \tag{23}$$

It is the most frequently used equation in EHL solution problems and it is found from considerations of continuity. It is supposed that lubricant travels through cavitation region in streams, separated by bubbles. Separation starts at the point of cavitation, hence, at this point velocity profile of the lubricant is linear. Immediately before cavitation region, velocity profile obeys Reynolds equation, and hence gives nonlinear distribution, if pressure gradient is not zero. Thus, only pressure gradient equal to zero can satisfy these considerations.

One way of cavitation boundary implementation is known as penalty method, introduced by Wu (Wu 1986). Consider following form of Reynolds equation:

$$\frac{\partial}{\partial x}\left(\frac{\rho h^3}{12\mu}\frac{\partial p_c}{\partial x}\right) - u_m\frac{\partial(\rho h)}{\partial x} - \frac{\partial(\rho h)}{\partial t} - \frac{1}{\varepsilon}p_c^- = 0 \tag{24}$$

where $p_c^- = \min(0, p_c)$. It was shown by Wu:

$$\lim_{\varepsilon \to 0} p_c(x) = p(x), \ \forall \ x$$

where $p(x)$ is the solution of the following system:

$$\begin{cases} \dfrac{\partial}{\partial x}\left(\dfrac{\rho h^3}{12\mu}\dfrac{\partial p}{\partial x}\right) - u_m\dfrac{\partial(\rho h)}{\partial x} - \dfrac{\partial(\rho h)}{\partial t} = 0 \\ \dfrac{\partial p}{\partial x}\bigg|_{x_c} = 0 \end{cases} \tag{25}$$

Thus, the cavitation boundary condition can be implemented through the solution of equation (24). This approach is used in the thesis.

3.9. Full system of equations

Finally, it is possible to write down the system of equations fully describing the examined problem.

$$\begin{cases} \dfrac{\partial}{\partial x}\left(\dfrac{\rho h^3}{12\mu}\dfrac{\partial p}{\partial x}\right) - u_m\dfrac{\partial(\rho h)}{\partial x} - \dfrac{\partial(\rho h)}{\partial t} = 0 \\[2mm] F_l = \displaystyle\int_{-\infty}^{x_c} p(x')dx' \\[2mm] h(x,t) = h_0(t) + \dfrac{x^2}{2R} + h_e(x,t) + h_w(x,t) - s(x,t) \end{cases} \qquad (26)$$

Boundary conditions:

$$\begin{cases} p(-\infty) = p_0 \\[2mm] p(x_c) = p_0 \\[2mm] \left.\dfrac{\partial p}{\partial x}\right|_{x_c} = 0 \end{cases} \qquad (27)$$

where

$$\begin{cases} h_e(x,t) = -\dfrac{4}{\pi E'}\displaystyle\int_{x_a}^{x_c} p(x',t)\ln(x - x',t)\,dx' + C(t) \\[2mm] h_w(x + ut, t) = k_w u \displaystyle\int_0^t p(x + ut', t')dt' \\[2mm] s(x) = A_m\sin(\lambda x) \end{cases} \qquad (28)$$

and

$$\mu(p) = \mu_0\exp(\alpha p) \qquad (29)$$

System of equations (26) - (29) includes all equations necessary to solve.

3.10. Dimensional equations

It is convenient to study instead of actual parameters, dimensionless ones. To perform this procedure, following dimensionless variables are introduced.

$$p - P_0 = \bar{p}P_0, \quad x = \bar{x}R, \quad h = \bar{h}R, t = \frac{R}{u_m}\bar{t}, \quad k_w = \frac{\overline{k_w}}{P_0}, \bar{\mu} = \frac{\mu}{\mu_0}, \bar{\alpha} = \alpha P_0$$

$$s = \bar{s}R, A_m = \overline{A_m}R, F_l = RP_0\overline{F_l}$$

Substitution of these variables gives the dimensionless equations:

$$\begin{cases} \dfrac{\partial}{\partial\bar{x}}\left(A\dfrac{\bar{\rho}\bar{h}^3}{\bar{\mu}}\dfrac{\partial\bar{p}}{\partial\bar{x}}\right) - \dfrac{\partial(\bar{\rho}\bar{h})}{\partial\bar{x}} - \dfrac{\partial(\bar{\rho}\bar{h})}{\partial\bar{t}} = 0 \\ \overline{F_l} = \displaystyle\int_{-\infty}^{\overline{x_c}}\bar{p}(\bar{x}')d\bar{x}' \\ \bar{h}(\bar{x},\bar{t}) = \bar{h}_0\,(\bar{t}) + \dfrac{\bar{x}^2}{2} + \bar{h}_e(\bar{x},\bar{t}) + \bar{h}_w(\bar{x},\bar{t}) - \bar{s}(\bar{x},\bar{t}) \end{cases} \qquad (30)$$

$$\begin{cases} \bar{p}(-\infty) = 0 \\ \bar{p}(\bar{x}_c) = 0 \\ \left.\dfrac{\partial\bar{p}}{\partial\bar{x}}\right|_{\bar{x}_c} = 0 \end{cases} \qquad (31)$$

where parameter $A = RP_0/12\mu_0 u_m$. Now it is possible to consider particular analytical solutions of the stated problem.

4. ANALYTICAL SOLUTIONS OF SIMPLIFIED PROBLEMS

In general, stated system of equations cannot be solved analytically, and only in a few simplified cases it is possible to obtain such a solution. Three stationary analytical solutions are discussed.

First case to consider is the lubrication of rigid bodies with constant viscosity and density. Although it is not applicable in most of the practical cases, it gives a closed form solution for a minimum film thickness and shows the relationship between parameters of the process.

As a second solution, Grubin's approximate formula is derived. This brilliant solution is also important to study due to account for viscosity-pressure variation and elasticity of contacting bodies.

Kapitsa solution of a point contact problem is discussed in the last section as the only analytical solution of three dimensional problems. It is derived for the case of rigid substrates, but takes into account viscosity- pressure variation. The price for this is the use of half-Sommerfeld boundary conditions.

4.1. Rigid body isoviscous solution

First, it is convenient to consider the simplest case of sliding motion in which bodies are assumed to be rigid. In this case, the system of equations simplifies to the following:

$$\begin{cases} \dfrac{\partial}{\partial \bar{x}}\left(A\bar{h}^3\dfrac{\partial \bar{p}}{\partial \bar{x}}\right) - \dfrac{\partial(\bar{h})}{\partial \bar{x}} = 0 \\[3mm] \bar{F}_l = \displaystyle\int_{-\infty}^{\bar{x}_c} \bar{p}(\bar{x}')d\bar{x}' \\[3mm] \bar{h}(\bar{x}) = \bar{h}_0 + \dfrac{\bar{x}^2}{2} \end{cases} \tag{32}$$

Regular boundary conditions (27) are applied.

Following variable substitution is applied:

$$\bar{x} = \sqrt{2\bar{h}_0}\tan \xi \tag{33}$$

Substitution of a new variable ξ into equations and double integration of the

Reynolds equation leads to a following system of equations on unknowns ξ_c and $\bar{h}_0$:

$$\begin{cases} \dfrac{A\bar{F}_l\bar{h}_0}{2} = f_1(\xi_c) \\[3mm] \dfrac{AC\bar{h}_0}{\sqrt{2\bar{h}_0}} = f_2(\xi_c) \end{cases} \tag{34}$$

$$\begin{cases} f_1(\xi_c) = \dfrac{1}{2}\left(1 + \dfrac{3}{4}C_1\right)\left(1 + \left(\xi_c + \dfrac{\pi}{2}\right)\tan\xi_c\right) + \dfrac{1}{8} \\[3mm] f_2(\xi_c) = \dfrac{1}{8}\left(1 + \dfrac{3}{2}C_1\right)\sin 2\xi_c + \dfrac{1}{2}\left(1 + \dfrac{3}{4}C_1\right)\left(\xi_c + \dfrac{\pi}{2}\right) \\[3mm] C_1 = -\dfrac{1}{\cos^2\xi_c} \end{cases} \tag{35}$$

Once ξ_c and $\bar{h}_0$ are known, pressure distribution is calculated according to

expression:

$$\bar{p}(\xi) = \dfrac{\sqrt{2\bar{h}_0}}{\bar{h}_0^{\,2}A}\left[\dfrac{1}{4}\sin 2\xi + \dfrac{\xi}{2} + C_1\left(\dfrac{1}{32}\sin 4\xi + \dfrac{1}{4}\sin 2\xi + \dfrac{3}{8}\xi\right) + \dfrac{3\pi}{16}C_1 \right.$$
$$\left. + \dfrac{\pi}{4}\right] \tag{36}$$

If the parameter $\bar{h}_0$ from the first of equations in (34) is expressed in terms of $f_1(\xi_c)$ and substituted into the second equation, the following relation is obtained:

$$\frac{1}{\sqrt{2}}\left(\frac{f_1(\xi_c)}{A\bar{F}_l}\right)^{\frac{3}{2}} = \frac{f_2(\xi_c)}{AC} \qquad (37)$$

This relation dictates the condition for functions $f_1(\xi_c)$ and $f_2(\xi_c)$ to be greater or equal to zero. In case if C – dimensionless cavitation pressure is zero, as in considered case, $f_2(\xi_c)$ must be equal to zero, as the left hand side is finite when $f_1(\xi_c)$ is greater than zero. Function $f_2(\xi_c)$ crosses zero only at one point $\xi_c = 0.4436$, thus, from the first equation of the system (34), $\bar{h}_0$ can be calculated as:

$$\bar{h}_0 = \frac{2f_1(\xi_c)}{A\bar{F}_l} = \frac{0.408}{A\bar{F}_l} \qquad (38)$$

Returning back to dimensional variables, final equation for a calculation of the minimum film thickness is obtained:

$$h_0 = 4.9\frac{\mu u_m R}{\bar{F}_l} \qquad (39)$$

This solution is known as Martin's theory approximation (Dowson D., Elasto-Hydrodynamic Lubrication. SI Edition. 1977), (Grubin A.N. 1949). Although it is well known that experimentally measured minimum film thicknesses for highly loaded contacts are much greater due to elastic deformation, this solution shows essential relationship of parameters in a hydrodynamic lubrication. Major conclusion in here is that higher viscosity lubricants produce thicker separation films.

4.2. Grubin's solution

As it is visible from the pressure-viscosity relation, viscosity of the lubricant increases exponentially with pressure. Thus, according to (39) minimum film thickness

will be increasing too. Based on this relation, Grubin was able to obtain an approximate analytical solution of the line contact problem.

Consider following system of equations:

$$
\begin{cases}
\dfrac{d}{dx}\left(\dfrac{\rho h^3}{12\mu}\dfrac{dp}{dx}\right) - u_m\dfrac{dh}{dx} = 0 \\[2mm]
F_l = \displaystyle\int_{-\infty}^{x_c} p(x')dx' \\[2mm]
\mu(p) = \mu_0\exp(\alpha p) \\[1mm]
p(-\infty) = 0
\end{cases}
\tag{40}
$$

Integrating once first equation, one can obtain:

$$
\frac{\rho h^3}{12\mu u_m}\frac{dp}{dx} = \frac{dh}{dx} + C
\tag{41}
$$

where C is a constant. At some point, pressure gradient equals to zero, and corresponding film thickness is noted as h'. If C is expressed through h', equation (41) takes form:

$$
\frac{dp}{dx} = 12\mu u_m\frac{h - h'}{h^3}
\tag{42}
$$

Introduce a variable $p_\mu = (1 - e^{-\alpha p})/\alpha$, and hence:

$$
\frac{d\,p_\mu}{dx} = 12\mu_0 u_m\frac{h - h'}{h^3}
\tag{43}
$$

Under conditions of heavily loaded constants considered by Grubin, pressure in contact gets very high, means goes to infinity and $p \to \infty$, which means $p_\mu \to \frac{1}{\alpha} = const$, $\frac{d\,p_\mu}{dx} = 0$. Therefore, inside of the contact film thickness is constant, and $h' = h_0$, where h_0 is the separation film thickness. Another conclusion from this statements is that pressure inside of the contact is the same as for the dry contact, as the lubricant is incompressible. Thus, the pressure distribution can be considered as Hertzian. From the other hand, Grubin

considered pressures outside of the contact zone as small, compared with inside, and therefore all deformations outside of it are due to pressure inside. Consequently, film thickness outside of Hertzian zone is written as:

$$h(x) = h_0 + \left(\frac{1 - \sigma_1^2}{E_1} + \frac{1 - \sigma_2^2}{E_2} \right) a p_{max} \delta \qquad (44)$$

where the latter term comes from Hertz theory, a is a half-width of Hertz contact and:

$$\delta = 2 \left\{ \frac{x}{a} \sqrt{\left(\frac{x}{a} \right)^2 - 1} - \ln \left[\frac{x}{a} + \sqrt{\left(\frac{x}{a} \right)^2 - 1} \right] \right\} \qquad (45)$$

For the line contact $p_{max} = \frac{2}{F_l}$. Introduce a new variable:

$$\frac{1}{E_l} = \left(\frac{1 - \sigma_1^2}{E_1} + \frac{1 - \sigma_2^2}{E_2} \right) \frac{1}{\pi} \qquad (46)$$

Then equation (44) can be written in a short way:

$$h(x) = h_0 + \frac{1}{E_l} F_l \delta \qquad (47)$$

As the film thickness is constant in contact zone, $h - h' = h - h_0 = \frac{1}{E_l} F_l \delta$. Thus, equation (43) gets form:

$$\frac{d p_\mu}{dx} = 12 \mu_0 u_m \frac{\frac{1}{E_l} F_l \delta}{\left(h_0 + \frac{1}{E_l} F_l \delta \right)^3} \qquad (48)$$

Now it is possible to re-write the last equation in a following form:

$$\frac{dp'_\mu}{dx'} = \frac{\delta}{H^3} \qquad (49)$$

and $p'_\mu = \left(\frac{F_l}{E_l}\right)^2 / 12\mu_0 u_m a$, $x' = x/a$. Integration from the negative infinity to -1, leads to an equation:

$$p'_\mu(-1) - p'_\mu(-\infty) = \int_{-\infty}^{-1} \frac{\delta}{H^3} dx \qquad (50)$$

Now the integration can be performed numerically for a range of H_0 and get an approximate expression:

$$p'_\mu(-1) = 0.0986 H_0^{-11/8} \qquad (51)$$

In the other hand, $p'_\mu(-1)$ must be equal to $1/\alpha$. Thus, substituting back all the variables, knowing from Hertz theory that $a = 2\sqrt{F_l R/E_l}$, h_0 can be obtained:

$$h_0^{11/8} = 2.3664 \frac{\mu_0 u_m \alpha \sqrt{R}}{F_l/E_l} \qquad (52)$$

Equation (52) is a result of a brilliant analysis of Grubin and as it was shown later, fairly matches experimentally measured film thicknesses for highly loaded contacts.

4.3. Kapitsa solution of point contact problem

In case of rigid bodies and half-Sommerfeld boundary conditions, a famous Russian scientist Kapitsa was able to obtain an analytical solution of point contact problem.

Assume a following pressure distribution:

$$p = \frac{kx}{h^2} \qquad (53)$$

Substitution of this expression into three dimensional stationary Reynolds's equation then gives:

$$-\frac{3kx}{R_x} - \frac{2kx}{R_y} = 12 u_m \mu \frac{x}{R_x} \qquad (54)$$

And thus, $k = -12u_m\mu/3 + 2\frac{R_x}{R_y}$. For balls, $R_x = R_y$, then pressure equals to:

$$p = -\frac{12}{5}\frac{u_m\mu x}{h^2}$$ (55)

From the load balance and half-Sommerfeld boundary conditions, one can obtain:

$$h_0 = \left(\frac{10.664u_m\mu R^{3/2}}{F_l}\right)^2$$ (56)

This solution is not frequently used. In details, derivation of Kapitsa and Grubin's solutions are well described in the book of Cameron (Cameron 1976).

5. NUMERICAL SOLUTION OF THE STATIONARY LINE CONTACT PROBLEM

First numerical calculations of a line EHL problem were performed by Dowson and Higginson (Dowson D., A Numerical Solution to the Elastohydrodynamic Problem 1959). Calculations in a wide range of parameters allowed them to derive a famous approximate formula for the film thickness. In their approach they used a simple Gauss-Seidel relaxation scheme. Later, improvements were done by other researchers to obtain solutions in high loaded contacts. In 1986 Lubrecht (Venner C.H. 2000) introduced multigrid approach and were able to reduce calculation time significantly. Further, Venner (Venner 1991) introduced multi-integration technique that made possible high load solutions to be obtained. First simultaneous solution using Newton-Raphson procedure was considered by Okamura (H. 1982), but further research in this direction was restricted by the nature of elastic deflection equation: elastic deflections of any point depends on the pressure all over the contact, which makes the resultant Jacobean matrix full. Solution of a system of linear equations with full matrix, necessary to solve in this case, requires much more computational sources. But relatively recently, differential deflection approach was introduced by Evans (Hughes 2000, Evans H.P. 1999) , where he found that the second derivative of elastic deflection is highly localized, and used it to build a numerical procedure for line and point contact problems. In the thesis, this approach was implemented for the line contact solution. Further, it will be discussed in details.

In general, there are two approaches for the solution of the stated problem. First is most frequently used, sequential, solves for all unknowns iteratively. Second approach,

fully implicit, and solves for unknowns simultaneously. This approach was abandoned by researchers at first, as it resulted in a full matrix of linear systems of equations. But as it was mentioned, this restriction could be overcome. Advantages and shortcomings of each method are listed in the Table 2.

Table 2. Comparison of solution approaches.

Sequential	Fully Implicit
Unknowns: p, h_0, x_c	
One of the unknowns is solved for, others are fixed	Unknowns are solved for simultaneously
Straightforward and simple Small storage capacity	Fast convergence rate
Slow convergence rate Unstable convergence for moderate and high loads	Full matrix of linearized system of equations Hard to implement cavitation condition Singular matrix for high loads

5.1. Discretization

In this section discrete equations are obtained using approximation schemes of different order. It should be noticed that several authors propose different schemes and approaches for approximations. Here the schemes employed by Ai (Ai 1993) are used.

5.1.1. Reynolds equation

Although a number of approximation schemes are available, the Poiseuillis term in Reynolds equation is usually approximated by a second order short central difference scheme:

$$\left(\frac{\partial}{\partial \bar{x}}\left(\xi\frac{\partial \bar{p}}{\partial \bar{x}}\right)\right)_i = \frac{\xi_{i+\frac{1}{2}}\left(\frac{\partial \bar{p}}{\partial \bar{x}}\right)_{i+\frac{1}{2}} - \xi_{i-\frac{1}{2}}\left(\frac{\partial \bar{p}}{\partial \bar{x}}\right)_{i-\frac{1}{2}}}{\Delta \bar{x}} \qquad (57)$$

where ΔX represents the mesh step size. The same discretization is applied for inner partial derivatives:

$$\left(\frac{\partial \bar{p}}{\partial \bar{x}}\right)_{i+\frac{1}{2}} = \frac{\bar{p}_{i+1} - \bar{p}_i}{\Delta \bar{x}} \qquad (58)$$

and

$$\left(\frac{\partial \bar{p}}{\partial \bar{x}}\right)_{i-\frac{1}{2}} = \frac{\bar{p}_i - \bar{p}_{i-1}}{\Delta \bar{x}} \qquad (59)$$

Substitution of (3.12) and (3.13) into (3.11) leads to the following final approximation:

$$\left(\frac{\partial}{\partial \bar{x}}\left(\xi\frac{\partial \bar{p}}{\partial \bar{x}}\right)\right)_i = \frac{\xi_{i+\frac{1}{2}}\bar{p}_{i+1} - \bar{p}_i(\xi_{i+\frac{1}{2}} + \xi_{i-\frac{1}{2}}) + \xi_{i-\frac{1}{2}}\bar{p}_{i-1}}{\Delta \bar{x}^2} \qquad (60)$$

where

$$\xi_{i\pm\frac{1}{2}} = (\xi_i + \xi_{i\pm 1})/2, \qquad (61)$$

$$\xi_{i\pm\frac{1}{2}} = \frac{\bar{\rho}_{i\pm\frac{1}{2}}\bar{h}^3_{i\pm\frac{1}{2}}}{\bar{\mu}_{i\pm\frac{1}{2}}} \qquad (62)$$

and

$$\bar{h}_{i\pm\frac{1}{2}} = (\bar{h}_i + \bar{h}_{i\pm1})/2 \tag{63}$$

Density and viscosity follow the same way as h in (63).

As well as Poiseuillis term, Couette term should be a second order of accuracy, although the first order is used too (Ai 1993). Venner (Venner C.H. 2000) proposed several second order schemes: short central order central, long central second order and second order upstream approximations. Second order upstream approximation is suggested for EHL problems to apply for entire domain a first order upstream discretization on the boundary.

He noticed that for low loads or pressure independent film thickness, any second order approximation is suitable. For the simplicity, here the following scheme was taken:

$$\left(\frac{\partial(\rho\bar{h})}{\partial\bar{x}}\right)_i = \frac{\bar{\rho}_{i+1}\bar{h}_{i+1} - \bar{\rho}_{i-1}\bar{h}_{i-1}}{2\Delta\bar{x}} \tag{64}$$

The time derivative term is approximated using first order implicit Euler's scheme:

$$\left(\frac{\partial(\bar{\rho}\bar{h})}{\partial\bar{t}}\right)_i = \frac{\bar{\rho}_i\bar{h}_i - \left(\bar{\rho}_i\bar{h}_i\right)^n}{\Delta\bar{t}} \tag{65}$$

The superscript n means that this value is taken from the current time step. From now on, all the values from current time step will get superscript n, and from the next time step won't have any superscripts.

Gathering discretized equations and substituting into the first dimensionless equation of the system (30), leads to:

$$A\frac{\xi_{i+\frac{1}{2}}\bar{p}_{i+1} - \bar{p}_i(\xi_{i+\frac{1}{2}} + \xi_{i-\frac{1}{2}}) + \xi_{i-\frac{1}{2}}\bar{p}_{i-1}}{\Delta\bar{x}^2} - \frac{\bar{\rho}_{i+1}\bar{h}_{i+1} - \rho_{i-1}\bar{h}_{i-1}}{2\Delta\bar{x}}$$
$$- \frac{\rho_i\bar{h}_i - \left(\rho_i\bar{h}_i\right)^n}{\Delta\bar{t}} = 0 \tag{66}$$

Keeping in mind the penalty formulation (24), we can introduce following function and use it for numerical solution further:

$$f_i^p = A \frac{\xi_{i+\frac{1}{2}}\bar{p}_{i+1} - \bar{p}_i(\xi_{i+\frac{1}{2}} + \xi_{i-\frac{1}{2}}) + \xi_{i-\frac{1}{2}}\bar{p}_{i-1}}{\Delta\bar{x}^2} - \frac{\bar{\rho}_{i+1}\bar{h}_{i+1} - \rho_{i-1}\bar{h}_{i-1}}{2\Delta\bar{x}}$$
$$- \frac{\rho_i\bar{h}_i - (\rho_i\bar{h}_i)^n}{\Delta\bar{t}} - \frac{1}{\varepsilon}\bar{p}_c^-$$

(67)

5.1.2. Force balance equation

Force balance equation as well as Reynolds equation can be discretized in a several ways. Parabolic approximation of pressure is used by (Ai 1993) in each point and is considered by (Gohar 1988). Venner (Venner C.H. 2000) suggests a rectangular approximation:

$$\bar{F}_l = \Delta\bar{x} \sum_{i=1}^{N} \bar{p}_i$$

(68)

where N is the number of approximation nodes. The same way as in a previous section, function is introduced:

$$f_0^h = \bar{F}_l - \Delta\bar{x} \sum_{i=1}^{N} \bar{p}_i$$

(69)

5.1.3. Fluid film thickness equation

According to section Surface roughness3.5, film thickness equation can be written in a following form:

$$h(x) = h_0 + h_g(x) + h_e(x) + h_w(x) - s(x)$$

(70)

41

All terms are straightforward to represent in discretized form for each node. Elastic term, in general can be represented in a following form:

$$h_e(x_i) = \sum_k G_k^i p_k \qquad (71)$$

This form is usually used in EHL calculations. Coefficients G_k^i can be considered as weights of pressure in point k to the deflection in point i. It will be shown later, that coefficients G_k^i are decaying very slowly from the point of application. It means that deflection in every point strongly depends on pressures even far from the point of interest. For sequential schemes, this fact doesn't make any difference, as the resultant matrix of linear equations is derived from Reynolds equation and thus is going to be tridiagonal. But in case of fully implicit approach, Jacobean will be a full matrix, and is needed to be inverted. Inversion of a full matrix is a very expensive procedure and usually is not used. That is the reason of popularity of sequential approach in EHL theory.

However, recently, as it was mentioned, another approach was invented by Evans (Evans H.P. 1999). Instead of considering the deflection itself, he considered a second derivative of the deflection, and was able to come up with following representation:

$$\left. \frac{\partial^2 h_e}{\partial x^2} \right|_{x_i} = \sum_k g_k^i p_k \qquad (72)$$

Solution of a second order differential equation requires two boundary conditions. It's clear that at the left hand side, far from the contact, deflection must be equal to zero. On the right boundary, constriction can be calculated through equation (71). Thus, in dimensionless form:

$$\bar{h}_N = \bar{h}_0 + \frac{\bar{x}_N^2}{2} + d \sum_k G_k^N \bar{p}_k - \bar{s}_N \qquad (73)$$

Comparison of coefficients in equation (71) and (73) is shown in the Figure 13.
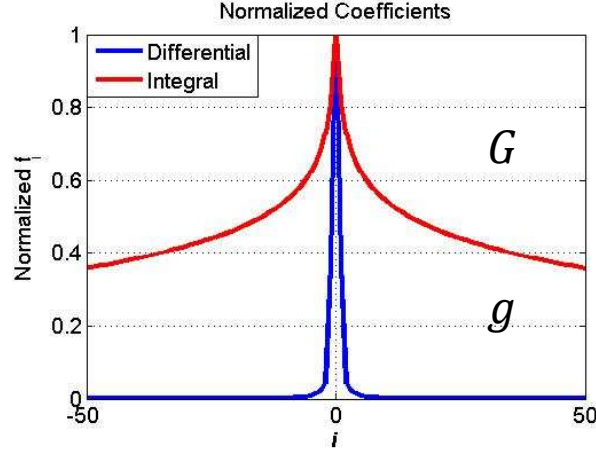
Figure 13. Dependence of coefficients on distance from point of application.

As we can see, the second derivative of elastic deflection is strongly localized. Thus, instead of considering the original film thickness equation, it is beneficial to work with its second derivative and consider the film thickness as an independent variable. Then, dimensionless form of the second derivative of the film thickness equation is written in a form:

$$\frac{\bar{h}_{i+1} - 2\bar{h}_i + \bar{h}_{i-1}}{\Delta X^2} = 1 + d \sum_k g_k^i \bar{p}_k$$

$$-\frac{\bar{s}_{i+1} - 2\bar{s}_i + \bar{s}_{i-1}}{\Delta X^2} + \frac{\bar{\omega}_{i+1} - 2\bar{\omega}_i + \bar{\omega}_{i-1}}{\Delta X^2}$$

(74)

It is possible to introduce following function:

$$f_i^h = \frac{\bar{h}_{i+1} - 2\bar{h}_i + \bar{h}_{i-1}}{\Delta X^2} - 1$$

$$-d \sum_k g_k^i \bar{p}_k + \frac{\bar{s}_{i+1} - 2\bar{s}_i + \bar{s}_{i-1}}{\Delta X^2} - \frac{\bar{\omega}_{i+1} - 2\bar{\omega}_i + \bar{\omega}_{i-1}}{\Delta X^2}$$

(75)

5.2. Newton's method

The key feature of the approach is to consider pressure and film thickness as independent variables. Thus, to obtain diagonally banded matrix, the vector of unknowns can be written in a following form:

$$\vec{V}_k = \begin{bmatrix} \bar{p}_2 \\ \bar{h}_2 \\ . \\ . \\ . \\ \bar{p}_{N-1} \\ \bar{h}_{N-1} \\ \bar{h}_N \\ \bar{h}_0 \end{bmatrix} \tag{76}$$

Thus, there are $2(N-1)+2$ unknown variables. For their solution, $2(N-1)+2$ equations (66),(68),(73),(74) are used.

According to Newton's method, following procedure is applied:

$$\vec{V}_{k+1} = \vec{V}_k - J^{-1}(\vec{V}_k)f(\vec{V}_k) \tag{77}$$

where $f(\vec{V}_k)$ is calculated from using previously introduced functions:

$$f = \begin{bmatrix} f_2^p \\ f_2^h \\ . \\ . \\ . \\ f_{N-1}^p \\ f_{N-1}^h \\ f_N^h \\ f_0^h \end{bmatrix} \tag{78}$$

Matrix of Jacobean must be calculated to solve equation (77). It is constructed in a following way:

$$
J = \begin{bmatrix}
\dfrac{\partial f_2^p}{\partial \bar{p}_2} & \dfrac{\partial f_2^p}{\partial \bar{h}_2} & \cdots & \dfrac{\partial f_2^p}{\partial \bar{p}_{N-1}} & \dfrac{\partial f_2^p}{\partial \bar{h}_{N-1}} & \dfrac{\partial f_2^p}{\partial \bar{h}_N} & \dfrac{\partial f_2^p}{\partial \bar{h}_0} \\[2ex]
\dfrac{\partial f_2^h}{\partial \bar{p}_2} & \dfrac{\partial f_2^h}{\partial \bar{h}_2} & \cdots & \dfrac{\partial f_2^h}{\partial \bar{p}_{N-1}} & \dfrac{\partial f_2^h}{\partial \bar{h}_{N-1}} & \dfrac{\partial f_2^h}{\partial \bar{h}_N} & \dfrac{\partial f_2^h}{\partial \bar{h}_0} \\[1ex]
\vdots & \vdots & & \vdots & & & \\[1ex]
\dfrac{\partial f_{N-1}^p}{\partial \bar{p}_2} & \dfrac{\partial f_{N-1}^p}{\partial \bar{h}_2} & \dfrac{\partial f_{N-1}^p}{\partial \bar{p}_{N-1}} & \dfrac{\partial f_{N-1}^p}{\partial \bar{h}_{N-1}} & \dfrac{\partial f_{N-1}^p}{\partial \bar{h}_N} & \dfrac{\partial f_{N-1}^p}{\partial \bar{h}_0} \\[2ex]
\dfrac{\partial f_{N-1}^h}{\partial \bar{p}_2} & \dfrac{\partial f_{N-1}^h}{\partial \bar{h}_2} & \dfrac{\partial f_{N-1}^h}{\partial \bar{p}_{N-1}} & \dfrac{\partial f_{N-1}^h}{\partial \bar{h}_{N-1}} & \dfrac{\partial f_{N-1}^h}{\partial \bar{h}_N} & \dfrac{\partial f_{N-1}^h}{\partial \bar{h}_0} \\[2ex]
\dfrac{\partial f_N^h}{\partial \bar{p}_2} & \dfrac{\partial f_N^h}{\partial \bar{h}_2} & \dfrac{\partial f_N^h}{\partial \bar{p}_{N-1}} & \dfrac{\partial f_N^h}{\partial \bar{h}_{N-1}} & \dfrac{\partial f_N^h}{\partial \bar{h}_N} & \dfrac{\partial f_N^h}{\partial \bar{h}_0} \\[2ex]
\dfrac{\partial f_0^h}{\partial \bar{p}_2} & \dfrac{\partial f_0^h}{\partial \bar{h}_2} & \dfrac{\partial f_0^h}{\partial \bar{p}_{N-1}} & \dfrac{\partial f_0^h}{\partial \bar{h}_{N-1}} & \dfrac{\partial f_0^h}{\partial \bar{h}_N} & \dfrac{\partial f_0^h}{\partial \bar{h}_0}
\end{bmatrix}
\tag{79}
$$

As it can be seen, if all coefficients of the deflection equation are used, then this matrix will be full. However, as it was shown, coefficients goes down rapidly, and hence, we can assume that only close neighbor points influence the second derivative of deflection in the point. In this case, J becomes banded and band width depends on how many neighbor points are considered.

5.3. Validation

In order to validate the proposed method, a number of comparisons were done. First, at the limit of infinite elastic modulus, numerical solution must be the same as for rigid cylinders. Thus, it is possible to compare analytical and numerical solutions for rigid case. Comparison is given in the Figure 14. Obviously, two solutions match. In the same figure, the effect of addition of elastic deflections is shown. The influence is very pronounced.
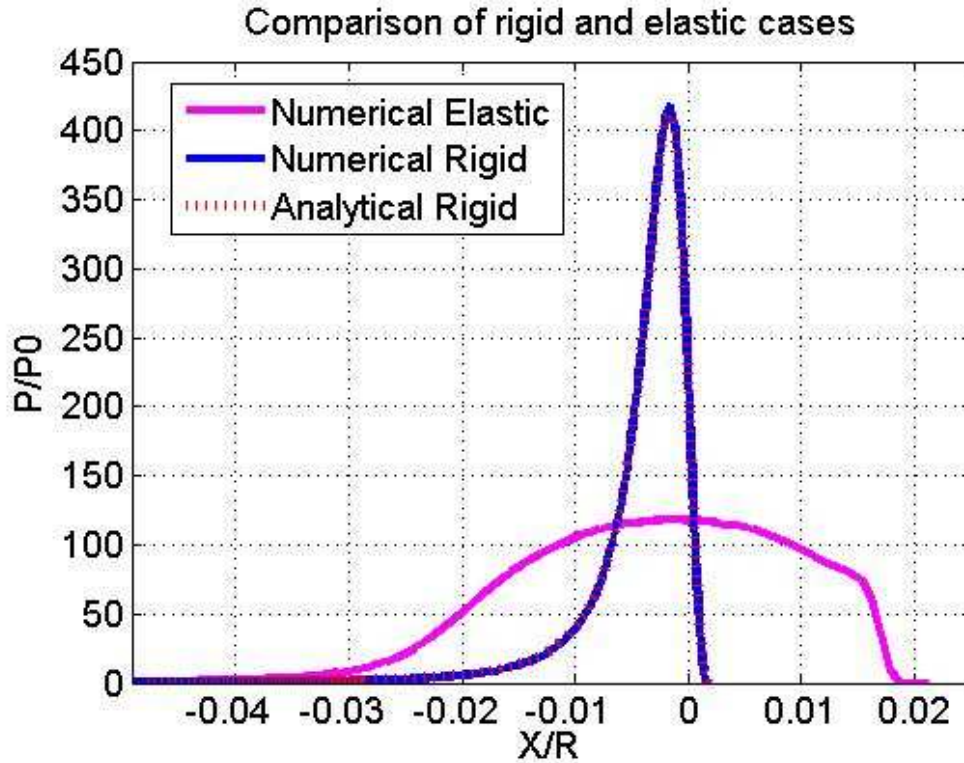
Figure 14. Comparison of numerical rigid case with analytical solution.

To validate numerical solution in case of elastic bodies, published data was used. Two independent sources were taken. Pressure and film thickness profiles were re-built from their papers using a ruler and compared with the results obtained in the thesis. First is the work by Okamura (H. 1982), who first had used Newton's method in EHL. In his solution, he considered the same line contact problem, however, the second-order differential Reynolds equation was first integrated and resulted a first order equation. This approach seems to be more accurate, because it reduces approximation errors of the second derivative. But this approach cannot be directly used for general 3D case, which makes it only particularly useful. In the Figure 15,Figure 16,Figure 17,Figure 18 comparison of pressure and film thicknesses with Okamura solution is shown. As it is seen, pressure distributions and film thickness profiles are consistent with reference data.
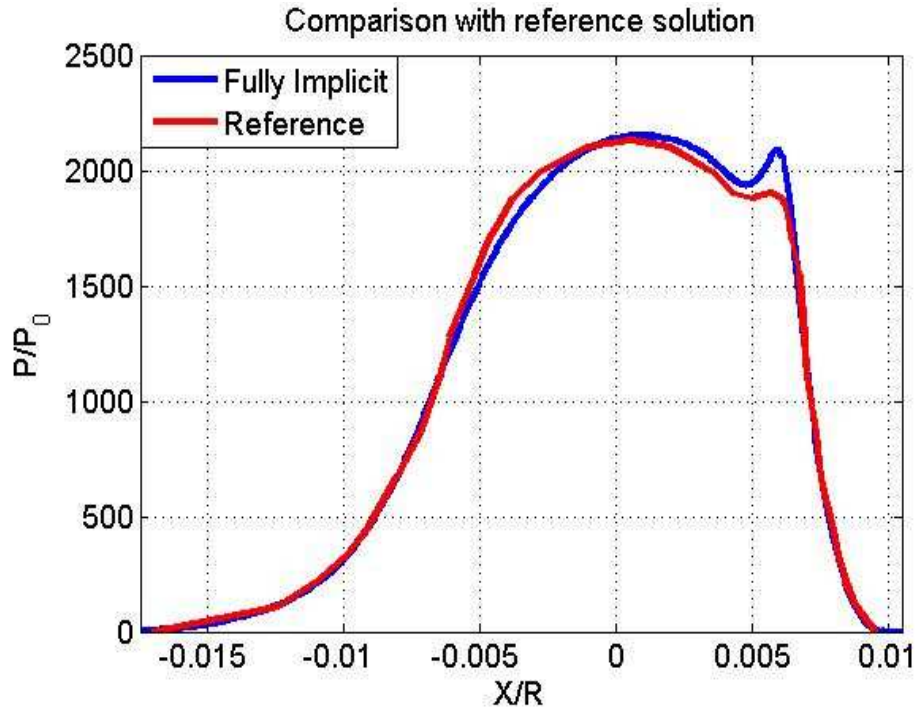
Figure 15. Comparison with Okamura. Pressure.
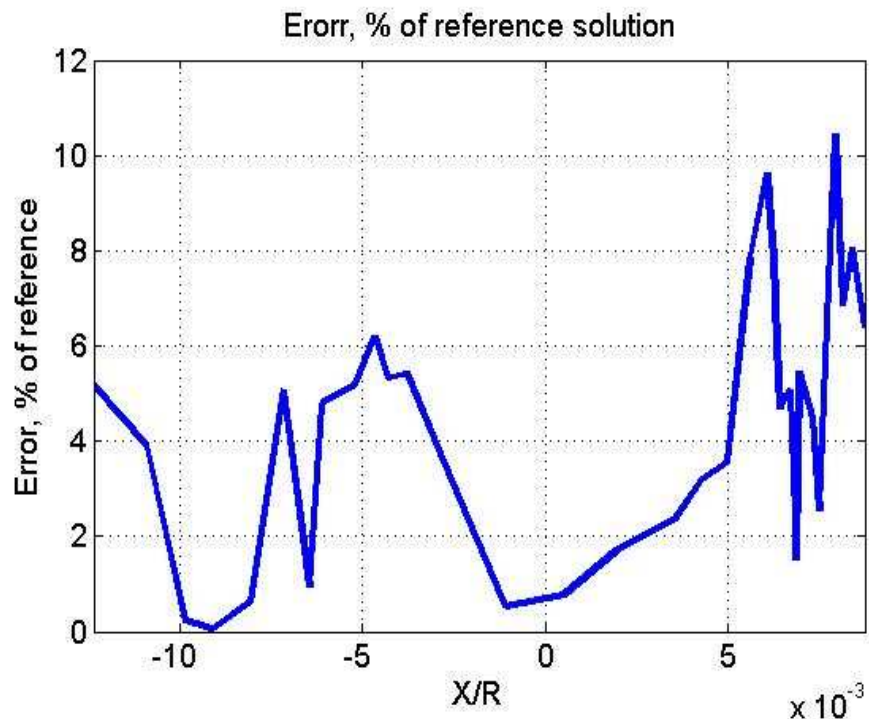
Figure 16. Relative error in pressure calculation, %, Okamura.

Figure 17. Comparison with Okamura. Film Thickness.

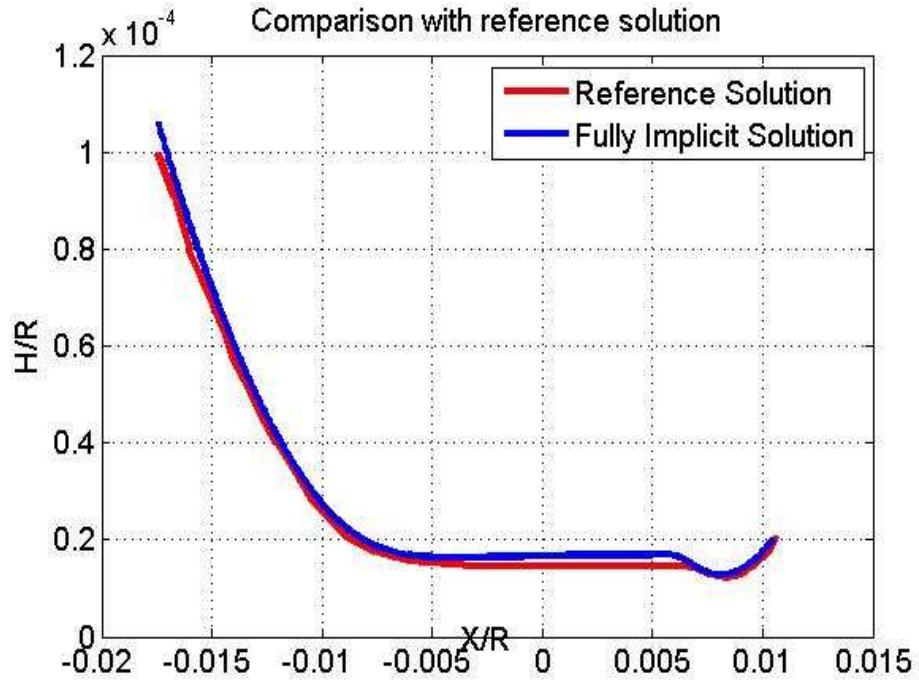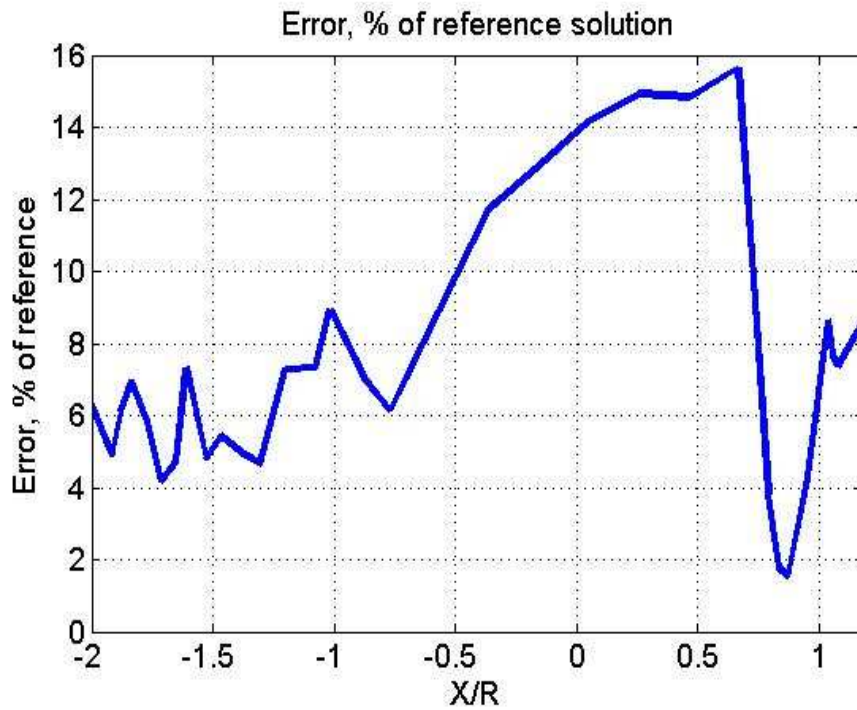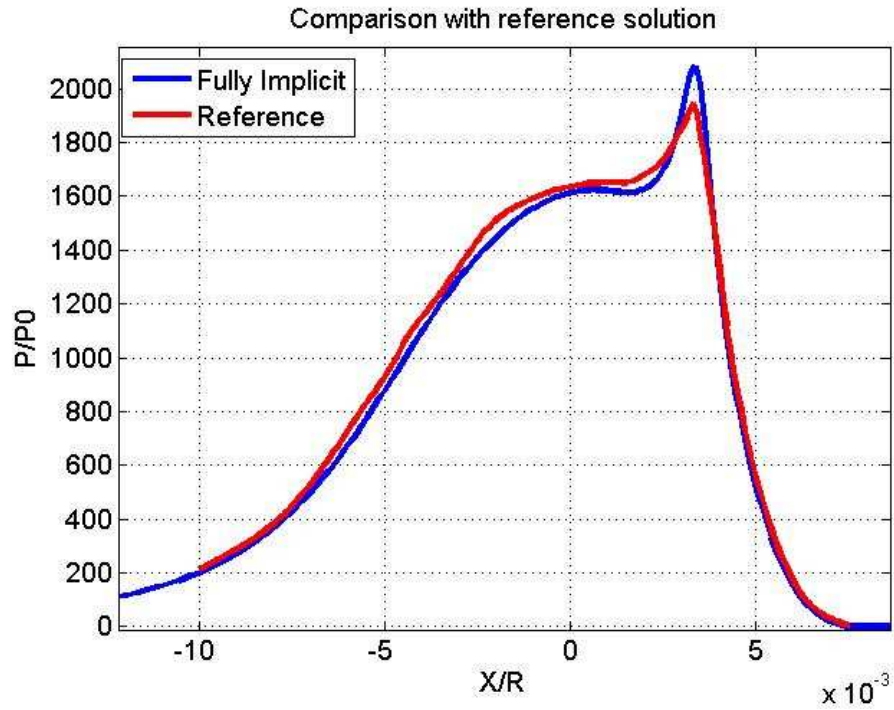Figure 18. Relative error in film thickness calculation, %, Okamura.
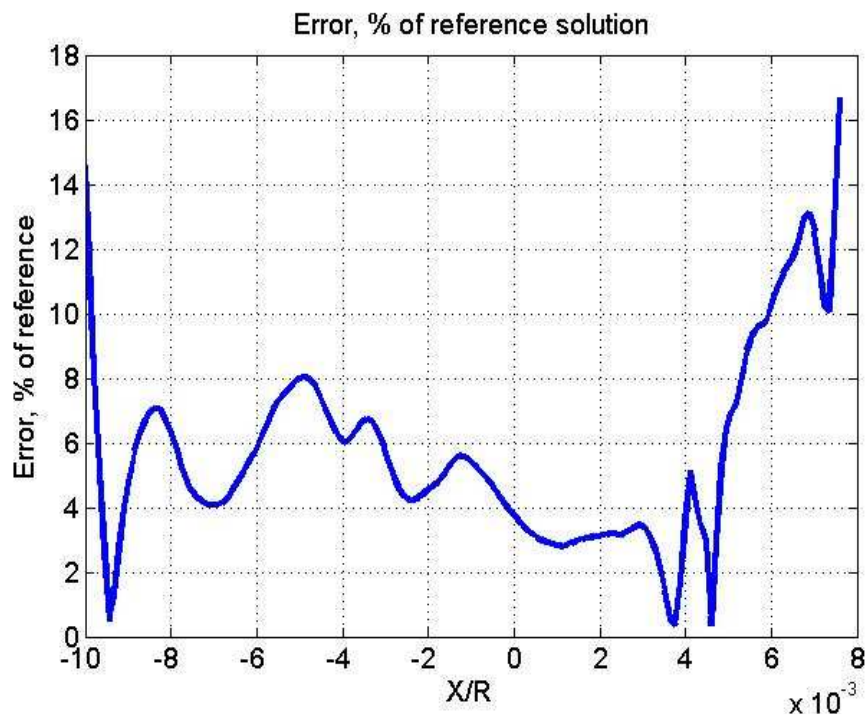
Figure 19. Comparison with Wu. Pressure.

Figure 20. Relative error in pressure calculation, %, Wu.

To ensure correctness of the developed numerical scheme, pressure distribution was

compared with another reference, namely, with solution obtained by Wu (Wu 1986).

Pressure distributions and relative errors are shown in Figure 19 and Figure 20. Again, it can be concluded that profiles are consistent. Thus, numerical solution by fully implicit approach is consistent with published data, and, hence, can be considered as correct. Solutions obtained by the solver will be used to analyze the stated problem of wear simulation.

5.4. Discussion of theoretical model

As it can be seen from the given solutions, there are several features in the EHL solution. It is worth to discuss them. First of all, if we consider the film thickness profile, we will definitely see the reduction of the film in the outlet of the contact. To analyze this fact, first consider red isoviscous curve in the Figure 21. At some point $\bar{x}$, pressure gradient is zero. Thus, the flow rate is fully determined by a linear part of velocity profile. At the outlet, according to Figure 22, there is a pressure gradient, which will increase velocity by addition of non-linear component. Thus, to fulfill the constant flow rate requirement, the linear part of velocity must decrease, and it is possible only if the gap height is decreased.

Further, consider the case of pressure dependent viscosity of lubricant. As it can be expected from the rigid theory, as viscosity increases, the film thickness increases, as it can be seen from the profiles. However, another feature to the film thickness profile is added, when viscosity changes. Right before closure of the film thickness at the outlet, a small bump occurs. It happens from the same considerations, when pressure gradient term is subtracted from velocity, gap has to be increased to fulfill the constant flow rate. After the peak pressure, the gradient again increases velocity, and the gap has to be decreased. As the pressure drop in this case is much more visible, the sharpness and deepness of the closure is more pronounced for the pressure dependent case, than for isoviscous case. The reasons

of pressure spike occurrence are not fully understood (Venner 1991). It is known that it occurs only for pressure-dependent viscosity model and for certain speeds, but researchers still cannot develop a full explanation. In the thesis, it was found that pressure spike occurs only when the Barus relationship is introduced.
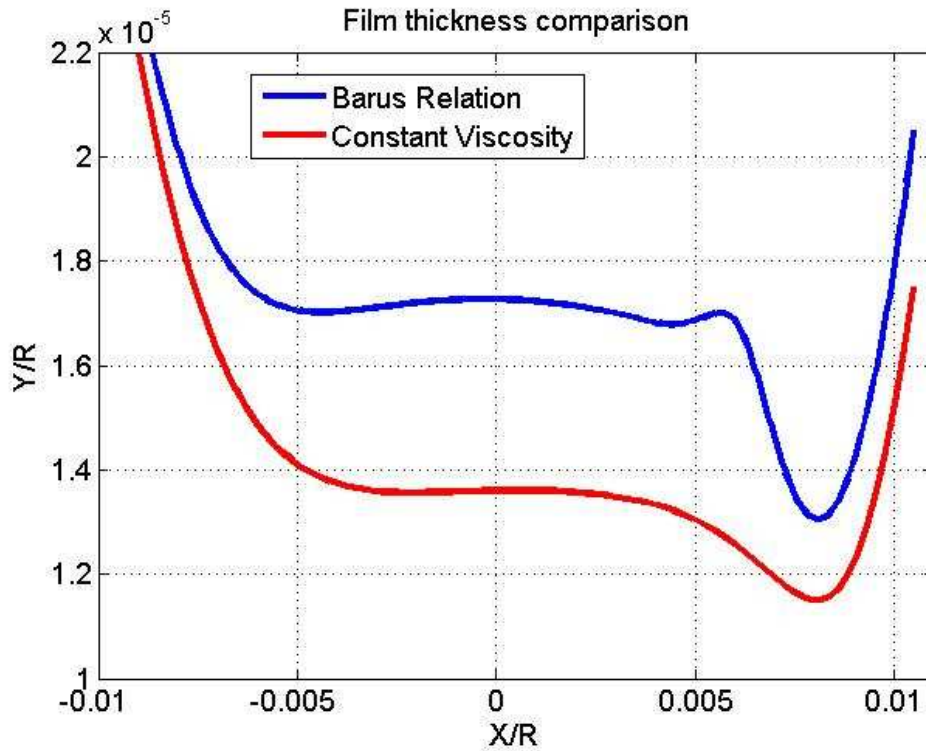
Figure 21. Film thickness for constant and pressure dependent viscosity.

It is worth to study dependence of pressure profile and film thickness on major parameters – speed and viscosity. To start with, pressure profiles for the case of given parameters were plot, and mean velocity was varied. It was varied around experimental value of 0.0079 m/s. In the Figure 23, number of such curves is given. Notation $U_m = 10$, means that the mean velocity is increased 10 times compared to experimental value of 0.0079. For comparison, Hertz solution for the dry case is also presented.
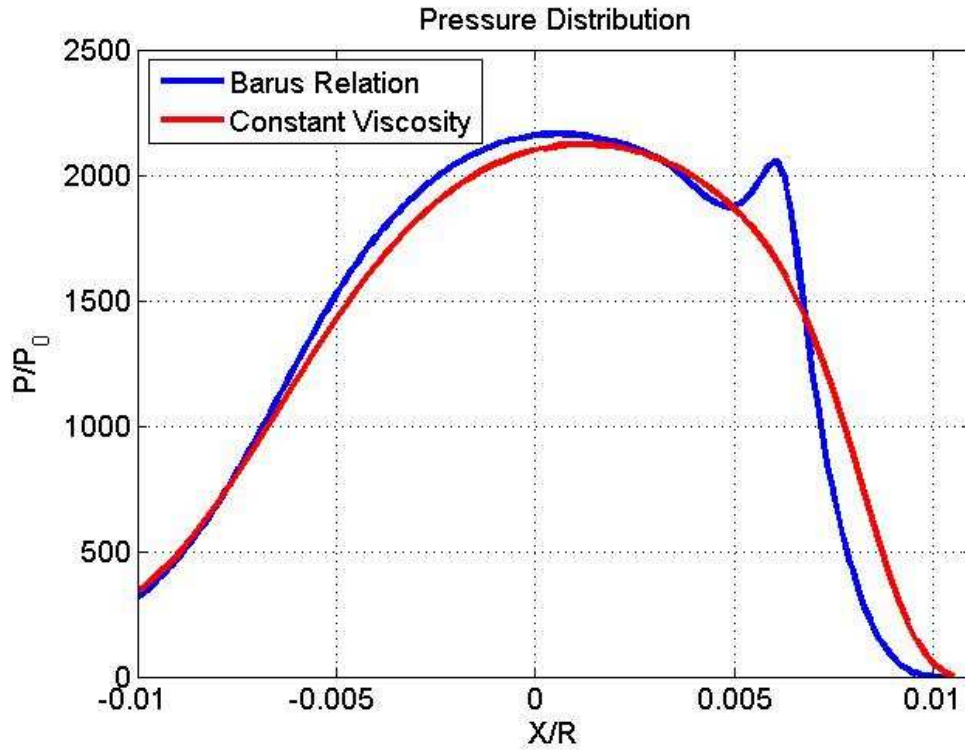
Figure 22. Pressure distribution for isoviscous and pressure dependent lubricant.
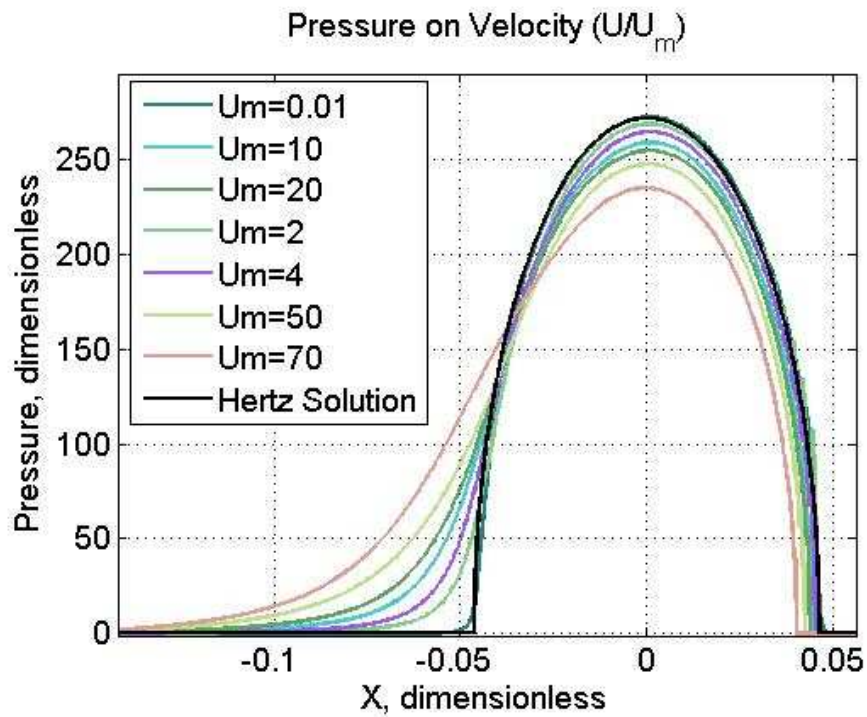
Figure 23. Dependence of pressure on the mean sliding speed.

As it can be readily seen, pressure spike did not occur for the speeds in considered range. For low speeds, pressure profile is very close to the Hertz solution profile, as there was no liquid at all. Increase in speed leads significant mismatch with dry case solution. Thus, at low speeds, the influence of lubricant flow to the pressure profile is small, and increases with speed. In general, it can be concluded that increase of speed results in decreased maximum pressure and smothered profile.

Corresponding film thickness profiles are shown in Figure 24. For low speeds, film thickness profile has a parallel section, width of which decreases with speed. When in pressure spike occurs, film thickness changes drastically, and the parallel section does not form. Further increase in speed leads to smoothening of the film, but with larger minimum thickness.
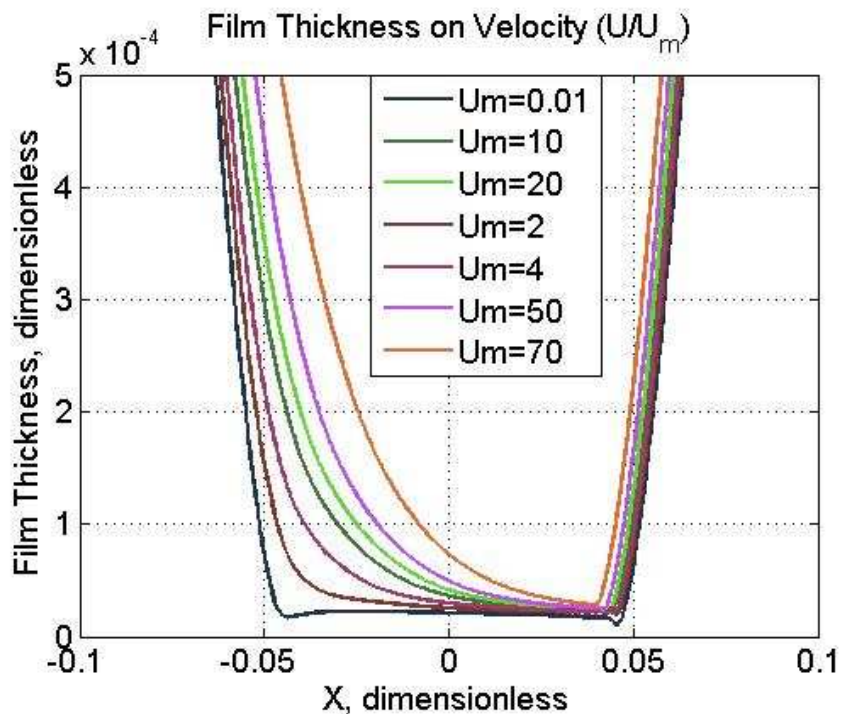
Figure 24. Dependence of film thickness on mean speed.

Next parameter to consider is the influece of viscosity. With all parameters fixed, viscosity of the lubricant was varied in the range from 1cP to 1000 cP. Hertz solution for

dry case was also drawn for comparison. According to Figure 25, for any viscosity in the range, pressure profiles are close to the Hertz solution.

Film thickness profiles presented in Figure 26, have a wide parallel section for low viscosities. With increase in viscosity this section reduces, with overal increase in minimum film thickness, which is shwon in Figure 27. Inportant observation here is that viscosity does not change the minimum film thickness, which is the separation distance between two bodies, significantly in the range of considered parameters. Thus, even 1000 times increase in viscosity will not guarantee a full separation of surfaces, when roughness is about 50-100 nm. In the other hand, for higher viscosities, the widht of the region where direct contact may occur is much narrower than for low viscosities, thus the total wear can be decreased. The same is actually true for changes in speed too.
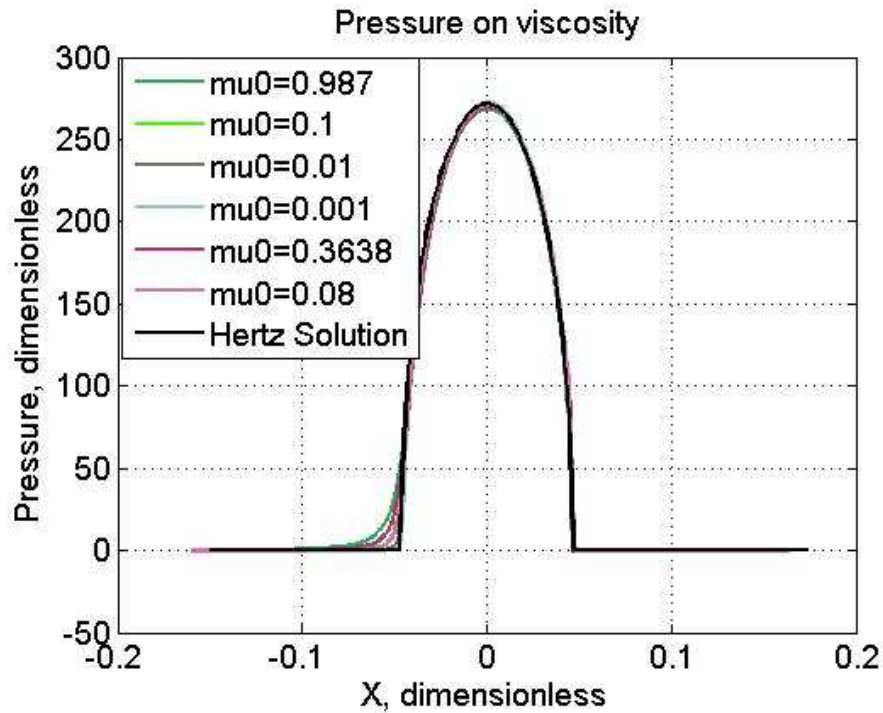
Figure 25. Dependence of pressure on viscosity.
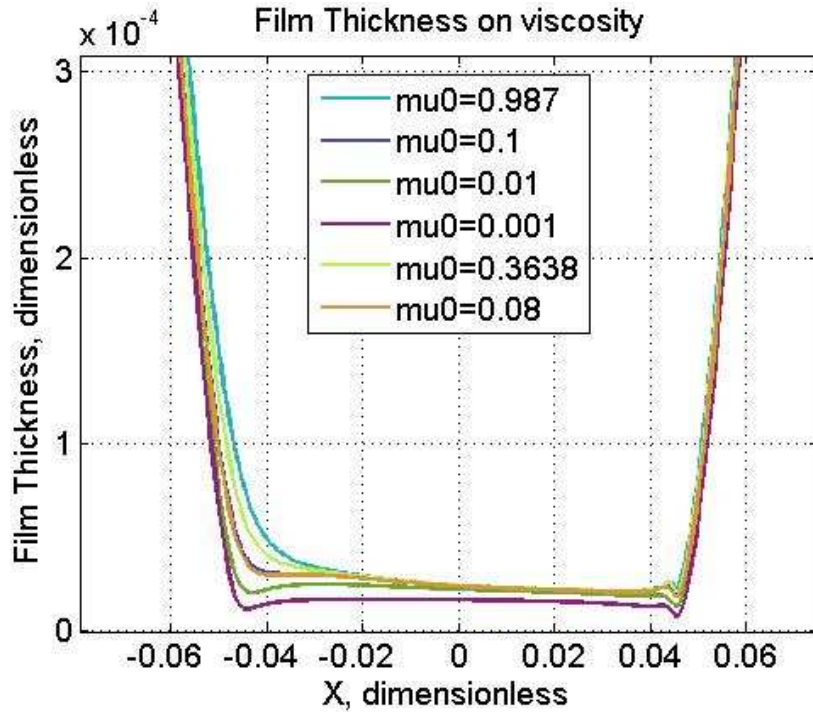
Figure 26. Dependence of film thickness on viscosity.
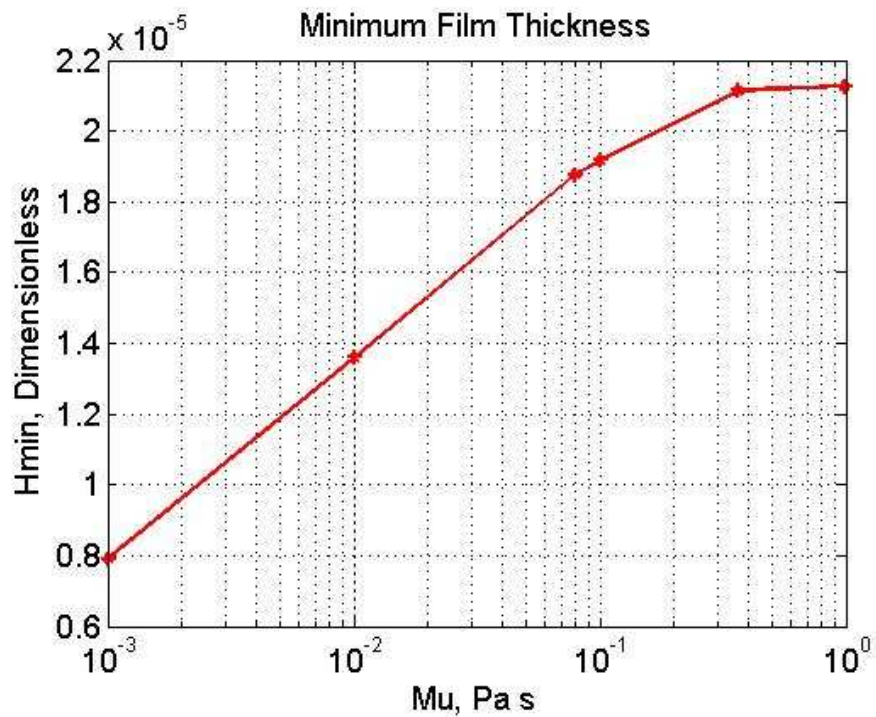
Figure 27. Dependence of minimum film thickness on viscosity.

It can be concluded from desrcibed calculations, that for the case of considered

parameters and elastically deformable substrates, influence of viscosity and speed on

minimum film thickness is not that important as for rigid case, although, these parameters changes profiles significantly.

6. EXPERIMENTAL MEASUREMENTS

Wear testing was performed under lubricated conditions using a pin-on-disc tribometer (CETR-UMT2). Schematic representation of it is shown in Figure 28. The polymer sample is fixed on a bottom of a lubricant filled holder, which is attached to a rotating disk. The counterpart steel ball is fixed in a ball holder. Controlled misalignment between central axis of the rotating disk and the ball holder makes the sliding path in a form of a circle with a certain diameter. During the test, friction force is measured by force sensors and friction coefficient is calculated. It is also possible to attach a thermocouple (k-type) and measure the temperature of the lubricant at some fixed point. The main controlled parameters are load, speed and duration.
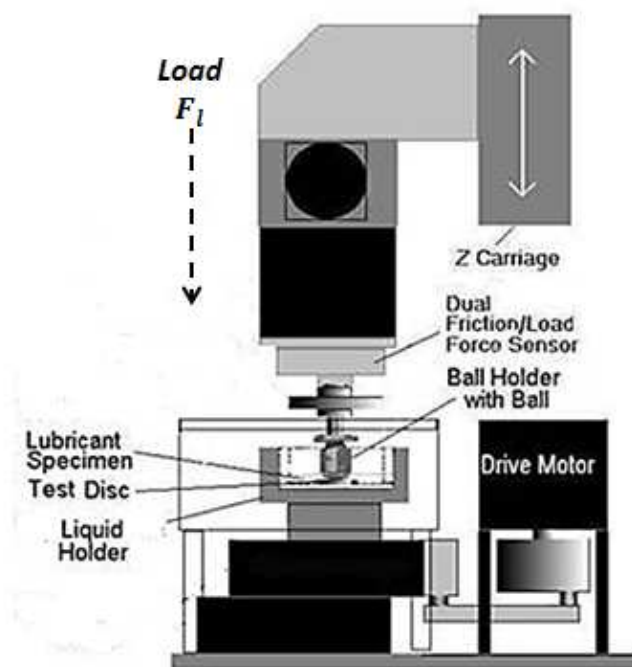
Figure 28. Schematic representation of a tribometer.

High Density Polyethylene was used as a wearing material. Each test specimen had a 1 in. × 1 in. square size and was fixed in a steel chamber filled with the lubricant. A

thermocouple was embedded into lubricant to record temperature change in the lubricant. Each sample was dried at temperature of 75 degrees Celsius for 12 hours before and after the test to exclude any moisture influence to mass measurements. Stainless steel balls (SS440 Grade 25) with diameter of 3/16 in. (4.762 mm) and surface roughness of 2 micro in. (0.0051 μm) from Salem Specialty Ball, Inc. were used. Most of the wear testing was performed under following conditions: normal load – 5 N, sliding velocity – 60 rpm, sliding diameter – 10 mm and duration – 4-8 hours. Friction force and friction coefficients as well as temperature of the lubricant in a chamber were recorded during the test. Mass wear loss was measured and used to evaluate wear rate.
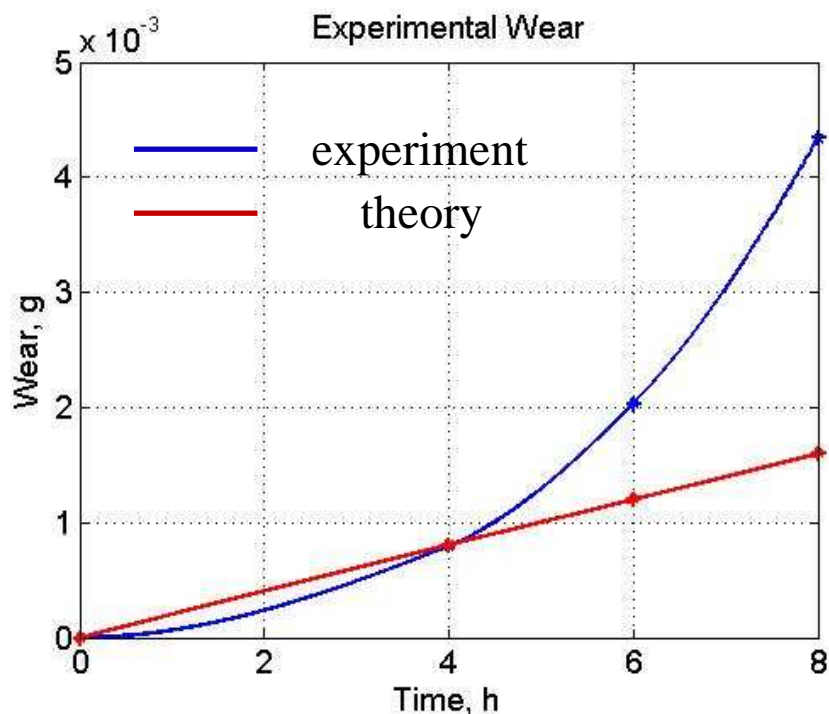
Figure 29. Wear of HDPE on time.

As lubricant, deionized water, glycerol and glycerol-water solutions were used. The reason for taking these lubricants is in their Newtonian behavior, even for high shear rates, encountered in EHL contacts.

In the Figure 29 the wear loss in grams is presented for the case of 95% weight glycerol-water solution. Corresponding data is given in Table 3. Asterisks represent actually measured values and line is the result of nonlinear interpolation. As it is easily seen, first four hours produce less wear than further hours. It means that wear is a nonlinear process. Increase in wear rate with time is related to the change of wear regime, from mild to more severe. Usually, after first four hours of wearing the track is smooth, only sometimes having rough cavities on the surface. However, after 8 hours, the track has rough surface, fully taken by cavities as it is shown in Figure 30. Thus, it is supposed that wear regime is changing in time. Theoretical modeling of wear in a proposed form only can be used for one regime, meaning that if coefficient of wear was found in mild regime, it cannot be applied to the estimation of wear in a severe regime. As it can be seen from the figure, the red line represent theoretically calculated wear rates based on the wear coefficient estimated from 4 hour long experiment. In this case, wear coefficient is low, $k_w = 10^{-15} \frac{m^3 N}{m}$, due to mild wear regime, thus it underestimates wear mass loss in other regimes.

Figure 30. Photographs of wear surface evolution in time.

Important experimental curve can be built if the wear is plot against viscosity of lubricant. For this purposes, dry, water lubricated, 95% glycerol-water solution and pure

glycerol were used as lubricants in 4 hour long tests. Experimental wear measurements then can be used to plot the graph Figure 31.

Table 3. Wear mass loss and standard deviation (95% glycerol-water mixture)

Time, hours	Mean Wear Loss, grams	Standard Deviation, grams
4	0.0008	0.0008
6	0.002	0.0018
8	0.004	0.0025
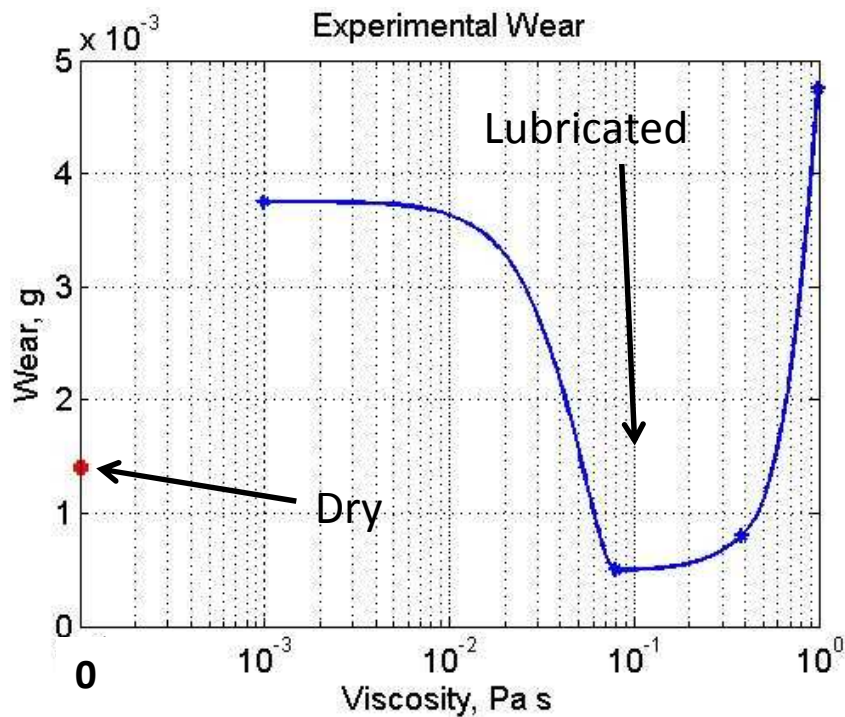
Figure 31. Dependence of worn mass on viscosity.

In the Figure 31 it is seen that the wear rate for dry condition is not highest. Further, for the case of water lubrication, the wear rate significantly increases. When the viscosity is increased till about 0.38 Pa s, the wear is dropped lower of the dry case. Further increase in viscosity leads to the increase in wear mass loss. Thus, it can be assumed, that the minimum wear loss under lubricated conditions will be in the range of viscosities starting from 1 cP to about 380 cP, and closer to latter. In general, the behavior is quite logical,

60

except of the low worn mass for the dry case. In the other hand, some researchers (Xu S. 2012) have shown that HDPE has outstanding self-lubrication properties in dry conditions. This theory implies that a thin film of HDPE is built in relative motion and protects the lower layers of HDPE from wearing.

Another important experimental measurement is friction coefficient. For the same tests, friction coefficient was measured. In case of 95% glycerol-water solution, friction coefficient is shown for all experiments in Figure 32. It is necessary to have a mean value of friction coefficient, thus, it is plotted in Figure 33. As it can be seen from these figures, friction coefficient decreases with time, and as long as the normal load is constant, it means that friction force decreases. It is common evidence, which indicates a running-in friction region. After it, most of the curves stabilize at some level and this value is of most interest. These values for different lubricants are summarized in Table 4. They were used to compare with theoretical calculations and discussions. Corresponding elevation in temperature is given in Table 5. These values were used for theoretical calculations as the estimation of the temperature in contact.

Viscosities of glycerol and glycerol-water solution were estimated using following correlation (Cheng 2008):

$$\mu_{mix} = \mu_{water}{}^{\gamma}\mu_{glycerol}{}^{1-\gamma} \qquad (80)$$

where γ is determined through volumetric concentrations of glycerol and water. It is necessary to notice that μ_{mix} depends on temperature, as both viscosities of water and glycerol depends on temperature.

$$\mu_{water} = 1.790exp((-1230 - T)T/(36100 + 360T)) \qquad (81)$$

and

$$\mu_{glycerol} = 12100exp((-1233 + T)T/(9900 + 70T)) \qquad (82)$$

In these equations temperature is measured in Celsius and viscosity is given in cP. The last term to identify here is γ:

$$\gamma = 1 - C + (abC(1 - C))/(aC + b(1 - C)) \qquad (83)$$

where C – mass concentration of glycerol in mixture, $a = 0.705 - 0.0012T$, $b = (4.9 + 0.036T)a\text{^}2.5$.
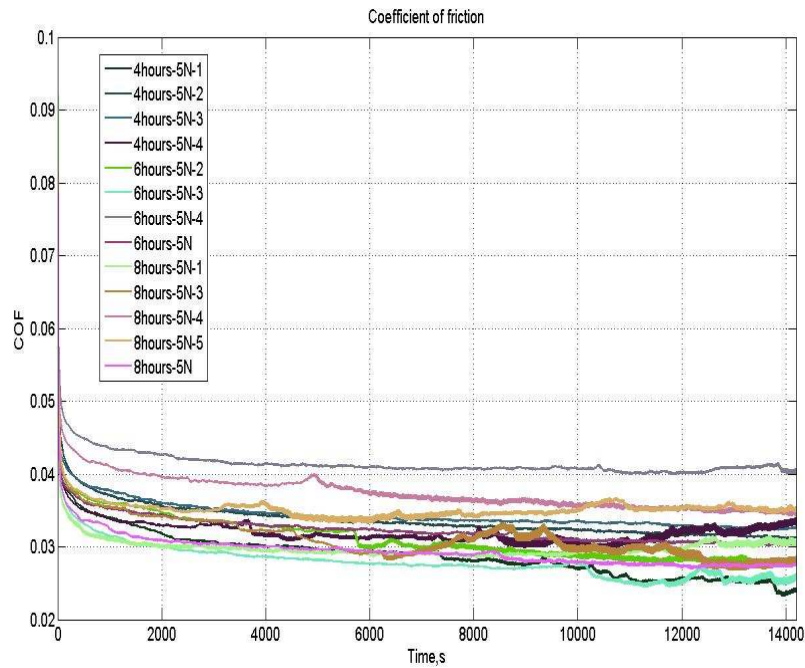
Figure 32. Friction coefficient measurements for 95% glycerol-water solution.

Temperature at the contact was taken as 24 degrees Celsius, Table 5. Thus, viscosity of pure glycerol equals to 987 cP and of 95% glycerol water solution equals to 363.8 cP. These values were used as an estimation of lubricant viscosity in a contact. For water, 1 cP was taken as it doesn't change significantly for assumed temperature.
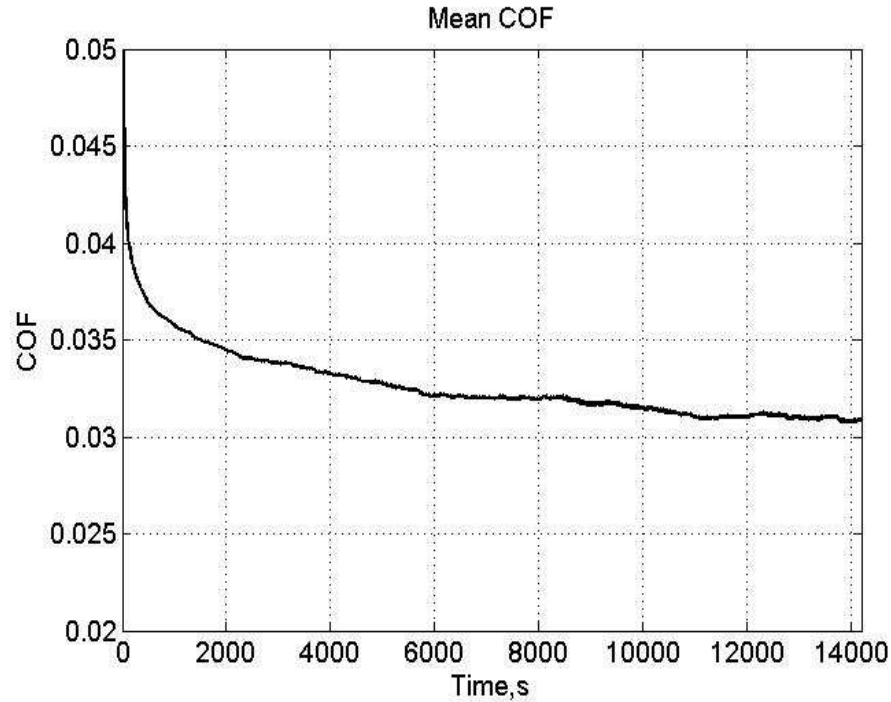
Figure 33. Mean friction coefficient for 95% glycerol-water solution.

Based on data provided in Table 4, it is possible to build a plot of dependence of friction coefficient on viscosity. This type of plot is called a Stribeck curve (Liu 2002) and usually it shows dependence of friction coefficient on product of initial viscosity and velocity. The following speculations are usually applied. When the distance between two rough surfaces is decreased from fully lubricated regime, asperities tend to form a contact and the friction is locally determined by shearing the boundary layers present at the surfaces. Further decrease will increase the friction and the load will be carried fully by the asperities and friction becomes of a Coulomb nature, i.e. independent of load and velocity. In the provided experiments, following curve can be plotted:
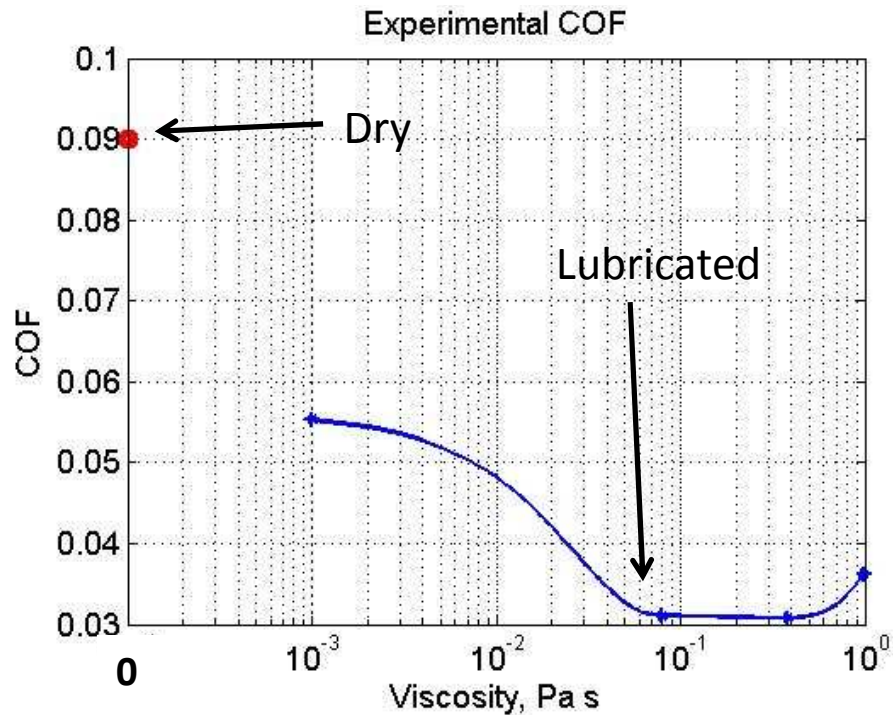
Figure 34. Dependency of friction coefficient on viscosity. Dry viscosity is taken as 0.

As it can be seen from the Figure 34, maximum coefficient of friction is developed for the dry case, which was expected. With addition of pure water, total friction coefficient is built by two components, dry and lubricated. As water viscosity is low, the minimum film thickness is extremely low and thus, the contribution of dry components is more pronounced, which results a high friction coefficient. Further, with increase of viscosity, the component of dry contact decreases, resulting decrease in total friction coefficient. With further increase in viscosity, dry component still decreasing, however, the lubricated component increases and at some viscosity the growth of it will compensate decrease in dry component and total friction coefficient will grow, as it is seen for a pure glycerol. This behavior misleadingly can be understood as an indicator of a full fluid lubrication regime, as it shows a typical relationship of friction and viscosity for fluids. However, as it will be shown from theoretical considerations, it is not true. This aspect will be discussed in a following section. In advance, it is worth to mention that for HDPE and steel contact for

the case of glycerol and considered load, radius of the ball, it is hard to achieve a full fluid lubrication regime by changing speed and viscosity, in the considered range.

Table 4. Coefficient of friction for different lubricants.

Lubricant	COF	Standard Deviation
Dry	0.09	N/A
Water	0.055	N/A
95% Glycerol	0.031	0.0043
Pure Glycerol	0.036	0.0027

Presence of dry component in friction also indicates that some part of the load is carried by asperities. It means, that pressure developed in the lubricant will be lower in reality, than calculated using a smooth surfaces theory and considering a full fluid lubrication regime.

To support the assumption of asperity contact, atomic force microscopy measurements of roughness of the HDPE surfaces before and after the test were taken. Roughness of the surface before the wear is shown in Figure 35 and after the 4 hours wear is shown in Figure 36. As it can be seen, initial surface is rough with mean roughness about 215 nm. During the test, the roughness is decreasing and after four hours, mean roughness is only 40 nm, as it can be seen in Figure 36. Forty nanometers is lower than predicted minimum film thickness, however, it is only mean value. It is also seen, that there are some areas on the surface of wear track, where the relative height is much larger than 52 nm, larger than 100 nm. These areas are considered to be asperities and come to direct contact with metal surface; hence, they are responsible for the dry component in friction and wear. Thus a mixed lubrication regime is encountered, and as it will be seen from the comparison

of experimental and theoretical calculation later, the full fluid lubrication regime is not encountered for the considered range of parameters.
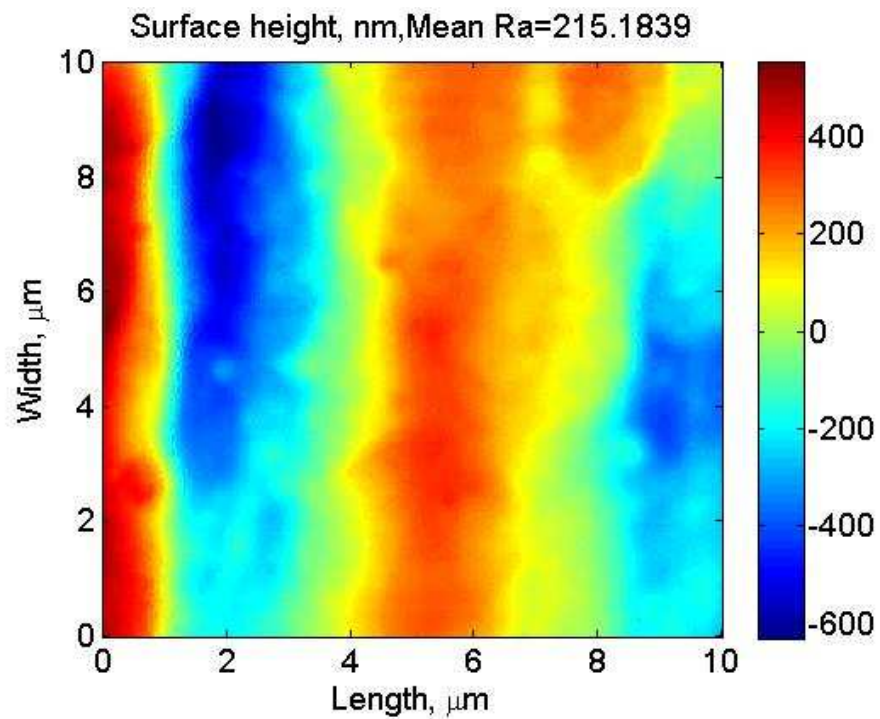
Figure 35. Surface roughness before wear.
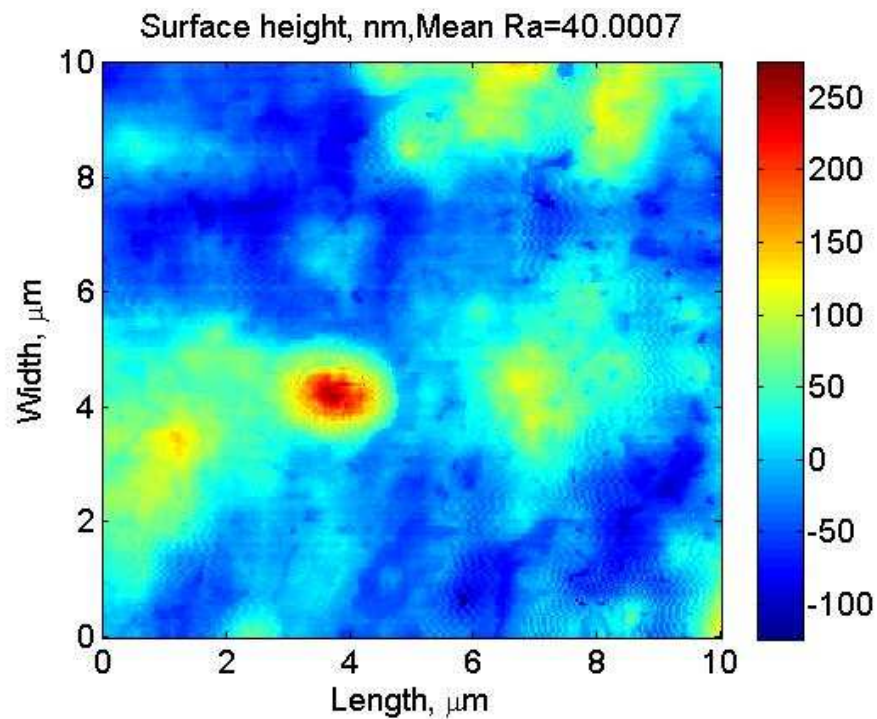
Figure 36. Surface roughness of the wear track after 4 hours.

Table 5. Mean temperature for different lubricants.

Lubricant	Temperature, C	Standard Deviation, C
Dry	22.9	N/A
Water	22.1	N/A
95% Glycerol	23.8	0.91
Pure Glycerol	24.1	0.33

7. THEORETICAL MODELING AND COMPARISON

WITH EXPERIMENT

First, parameters used in the theoretical calculations are summarized in Table 6.

Table 6. Properties in the system.

Load	5, N
Radius of the Ball	$2.5 \cdot 10^{-3}$, m
Um	0.0079, m/s
E(HDPE)	$1.05 \cdot 10^{9}$, Pa
α	$5.9 \cdot 10^{-9}$, 1/Pa
T	24 C

Necessary to notice that most of the time, ideally smooth surfaces are considered. Viscosities were varied in a range from 1 cP to 1000 cP. It is also important to re-scale a load from three dimensional experimental setup, to a two dimensional theoretical model. To accomplish it, the width of the wear track was measured after the test, and it was found to be about 1 mm. It was taken as constant for all calculations as a rough estimation. As long as width of the track is known, then it is easy to recalculate the length of the arc of the ball, bounded by a chord of 1 mm. This length was found to be equal $0.4R$ and taken as a scale factor for the load. Thus, force per unit length in direction perpendicular to the motion is $F_l = F/0.4R$, where the actual load is F.
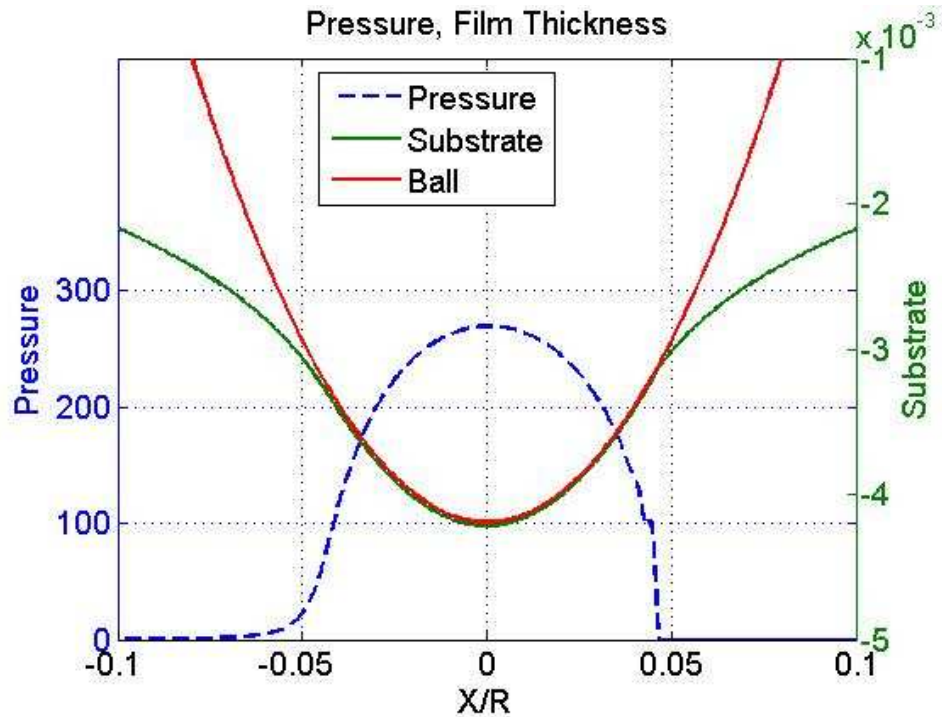
Figure 37. Computed pressure distribution and substrate.

The result of calculation for a standard set of parameters is shown in Figure 37 and Figure 38. As it can be seen, there is a pressure spike at the outlet of the pressurized region, although it is not very pronounced. Minimum film thickness for this case is equal to 52 nm. Thus, if ideally smooth case is considered and full fluid lubrication regime is assumed, then the separation film thickness is only 52 nm. Heights of the asperities of HDPE are most probably exceeding this value (direct contact), and even if not, considerably decreases this minimum distance, hence locally, high pressures may occur. For comparison, in fully lubricated steel contacts it is usually of micrometer orders.
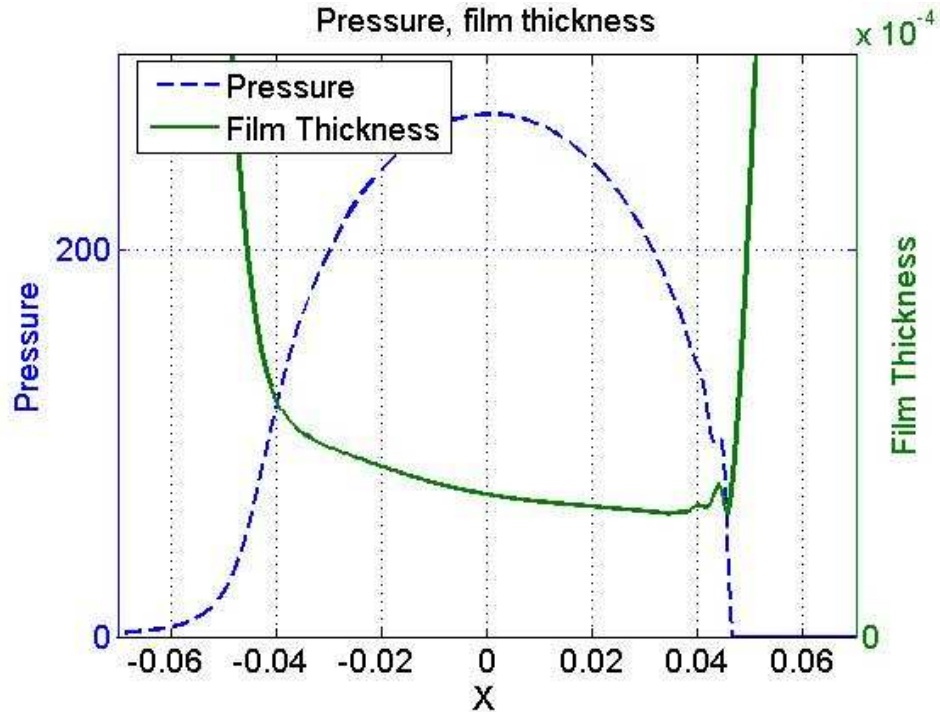
Figure 38. Pressure and film thickness.

Further, it is important to calculate friction coefficient for the modeled case and compare it with experiments. Dependence of theoretical friction coefficient on viscosity was explored and presented in Figure 39. As it can be assumed, the friction is determined by internal friction of liquid layers and thus, fully determined by viscosity of the lubricant. As it can be readily seen, friction coefficient is more than order of magnitude smaller for the viscosities of 363 and 987 cP when compared with experimental measurements. Based on this data and the fact that the minimum film thickness is 52 nm, it can be then concluded that the assumption of full fluid lubrication regime leads to underestimation of friction coefficient and hence, mixed lubrication is actually takes place. It means that part of the load is carried by liquid and part by direct contact, which will increase the total friction coefficient significantly. However, as it is seen from experimental curve in the Figure 34, friction coefficient highly dependent on viscosity of lubricant, and this fact is not yet clarified. The question can be stated, if the order of magnitude mismatch of calculated and

70

experimental friction coefficients is due to direct contact of the surfaces, why then increase in viscosity of lubricant in experiments shows significant impact to the measured coefficient of friction? This impact is again orders of magnitude higher than calculated through the theory.
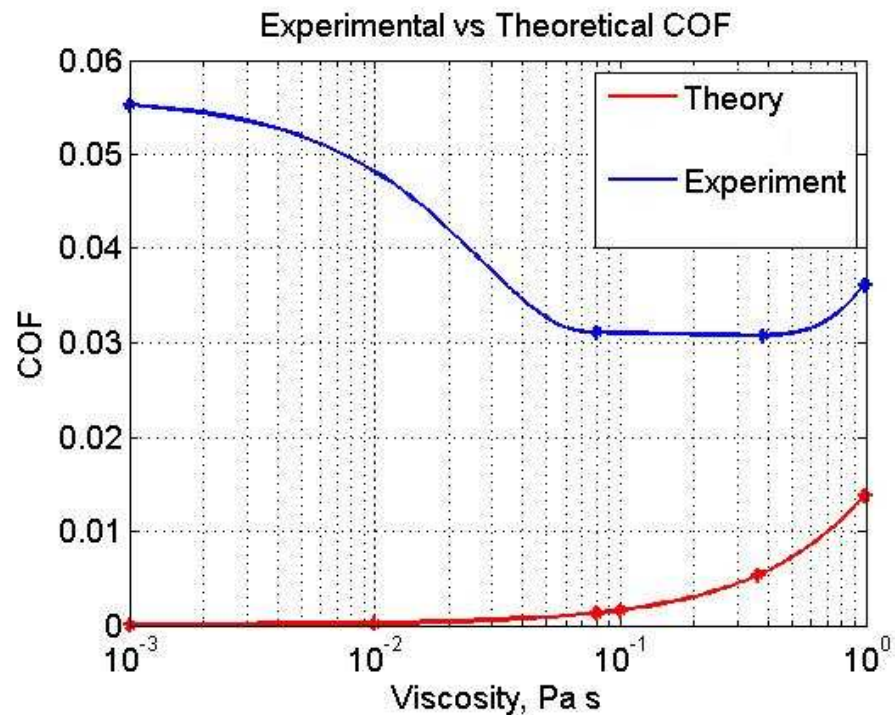
Figure 39. Comparison of theoretical and experimental friction coefficient on viscosity.

This question cannot be answered through calculations for ideally smooth surfaces. Hypothesized idea is that roughness of the surfaces can play a role there due to increased local pressure gradients, and, hence, shear strains. In case of steel contacts, pressures rises till 4000 atmospheres and up, this makes viscosity of lubricant to increase according to exponential law. For regular oil, pressure viscosity coefficient is usually about 4 times higher than for glycerol, thus, ensuring rise of viscosity by orders of magnitude in contact. These facts lead to high predicted friction coefficients and match with experimental data. In the considered case, pressure is only 250 atmospheres, and hence, there is no significant increase in viscosity. Thus, order of magnitude change in shear force can only be achieved

due to high pressure gradients or small film thickness. To explore this possibility, instead of ideally smooth surface of HDPE, the surface with one asperity with vicinity right under the ball tip was considered. Width of it was about 1 micrometer and height was varied. Corresponding change in minimum film thickness, pressure distribution and coefficient of friction were tracked.
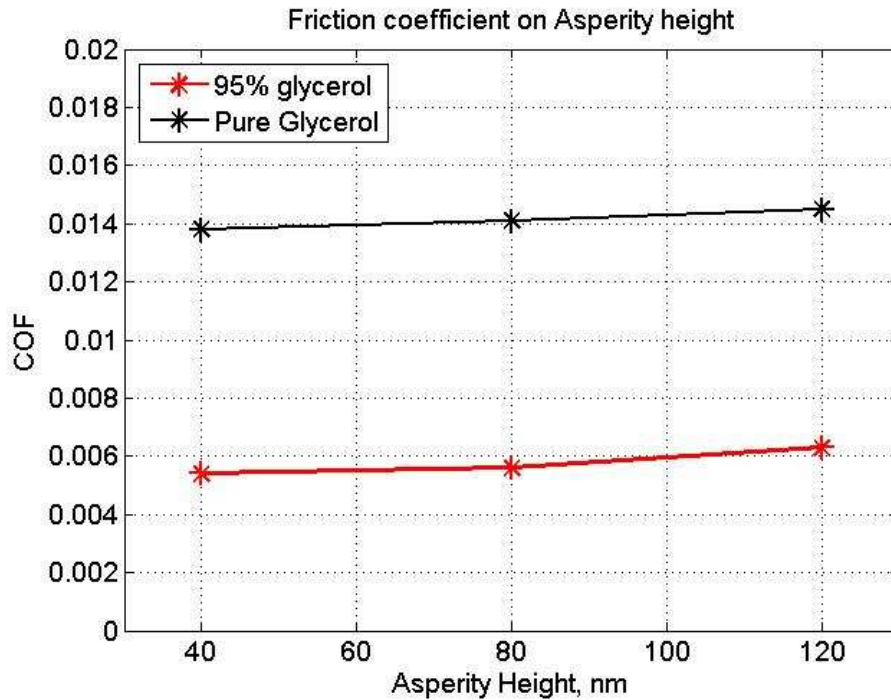
Figure 40. Asperity height and friction coefficient.

Comparison of Figure 39 and Figure 40 implies that addition of asperity significantly increases influence of viscosity on friction. At the same time, according to Figure 41, if the asperity height is enough, separation film thickness can get very low and direct contact may occur. Thus, friction coefficient will be increased. At the same time, if the viscosity of lubricant is increased, local friction around asperity is increased too, no matter whether direct contact occurs or not. However, calculated friction coefficient is still smaller than experimentally obtained. Thus, combination of dry friction and lubricated

friction only can give the experimentally recorded friction coefficient, with high dependence of friction on viscosity of lubricant.
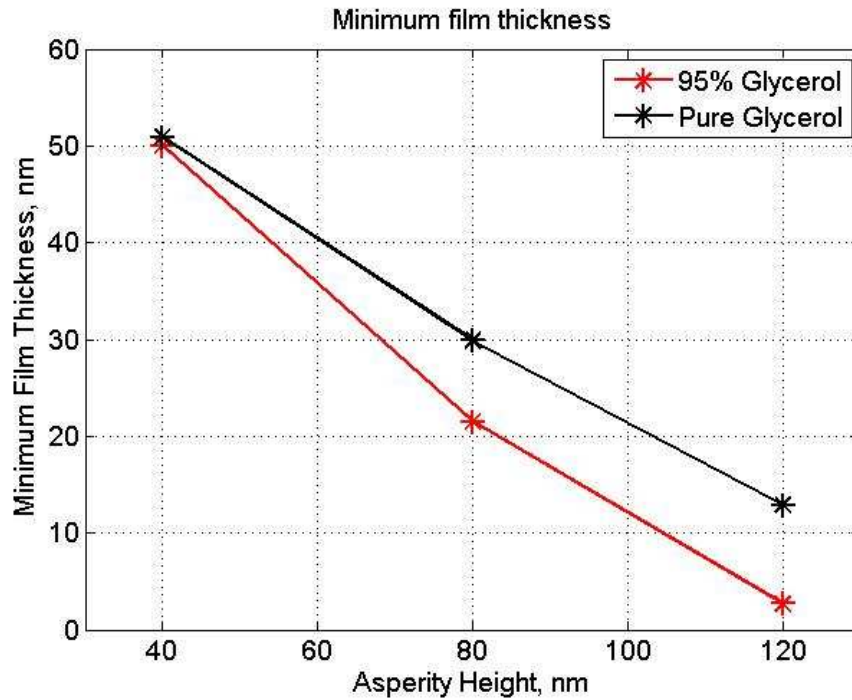
Figure 41. Dependence of minimum film thickness on asperity height.
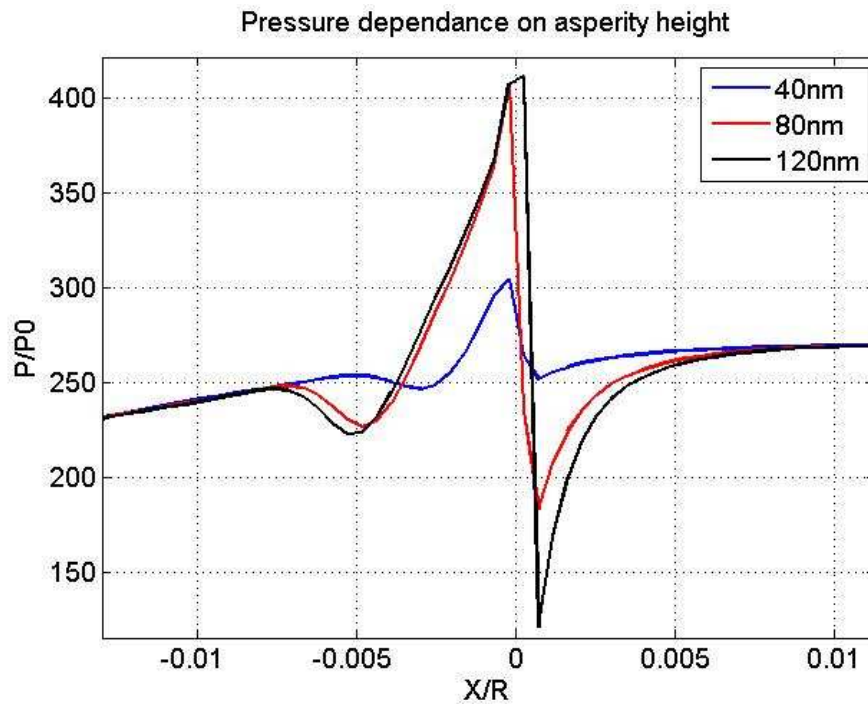
Figure 42. Pressure distribution around the asperity.

As it can be seen from Figure 42, anti-symmetrical pressure profile occurs at the vicinity of the asperity. This anti-symmetry is more pronounced for the higher asperity, and in limit will touch zero pressure value. If this happens, local cavitation may occur, thus, local low pressure zones can raise and in these zones no lubrication is provided, hence, condition of direct contact of the surfaces can be achieved. It can be speculated here, that these zones may be responsible for wear particle formation, their size and their morphology. As low pressure fields, surrounded by highly pressurized regions, these cavities may serve as a vacuum and an HDPE substrate locally may deflect inside of them. In the other hand, on the borders of cavities, high pressures are established; hence, high stresses may be experienced by HDPE particle trapped in cavity from both sides of cavity borders. Then the abrasive wear delamination of this part of HDPE can be formed and produce an HDPE wear particle.

8. WEAR PARTICLES

Wear debris of materials used nowadays in orthopedic replacements is known to be the major cause of failures in a long-term period. Recent studies showed that the autoimmune reaction to the foreign body is not only the consequence of the material itself, but also depends on the size and shape of the wear particles. Thus, the HDPE debris is worth to explore quantitatively and morphologically. Moreover, it can help in analysis of major wear mechanism. For these purposes, following experiment was undertaken. Wear testing was performed under phosphate buffered saline lubrication using a pin-on-disc tribometer (CETR-UMT2). Each test specimen had a 1 in. × 1 in. square size and was fixed in a steel chamber filled with the saline lubricant. The wear testing was performed under following conditions: normal load – 3 N, sliding velocity – 60 rpm, sliding diameter – 10 mm and duration – 8 hours. The wear debris was collected, isolated and characterized by scanning electron microscopy (SEM) at high magnifications and also by dynamic light scattering (DLS) particle sizing. The DLS measurements were in general consistent with the SEM observations. Small sphere-shaped wear particles of various diameters (predominantly less than 100 nm) were observed on the SEM images. The particles' diameter distributions obtained by the DLS technique also showed that the mean diameters of the majority of the particles were mostly less than 100 nm.

In the Figure 43, the small sphere shaped wear particles of HDPE are shown. Diameters are about only 100 nm, but these values are higher than predicted theoretical film thickness under employed parameters. In the Figure 45, the idealized Gaussian distribution of wear particle diameter is shown. As it can be seen, the mean diameter is

close to 50 nm, which roughly corresponds to SEM results.Figure 45. Idealized Gaussian distribution of wear particle diameter.
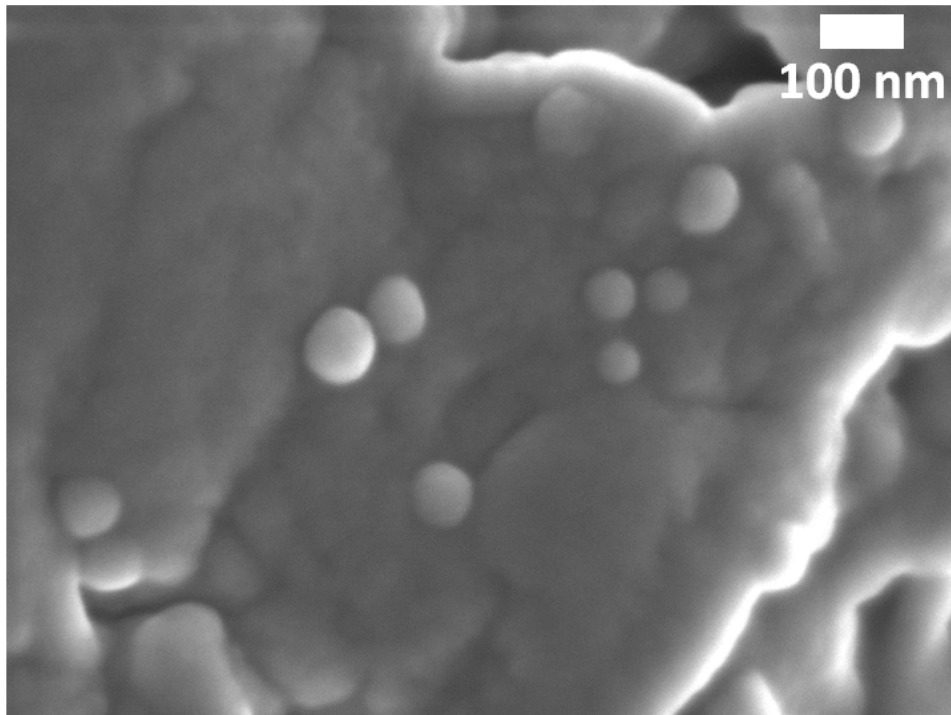
Figure 43. Sphere-shaped wear particles on the filter surface.

Calculated theoretical pressure distribution and film thickness for given parameters is shown in Figure 44. In this case, minimum film thickness is 52 nm, which is smaller, or at least of comparable size with observed wear debris particles. Thus, any of those particles passing under the ball will cause a direct contact of two surfaces and will be acting as a third body abrasive particle. As it is seen from the same figure, the region of small separation film thickness is quite wide, thus the effect of any particle will last through all this width. Thus, third body abrasive wear mechanism can be dominant in considered case.
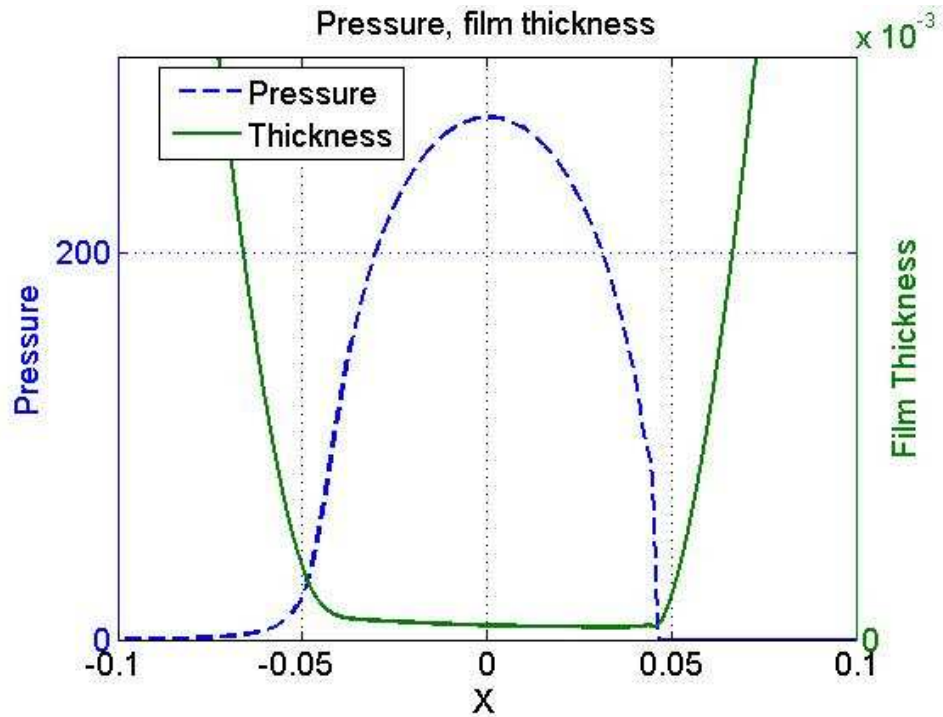
Figure 44. Pressure and film thickness for given parameters.
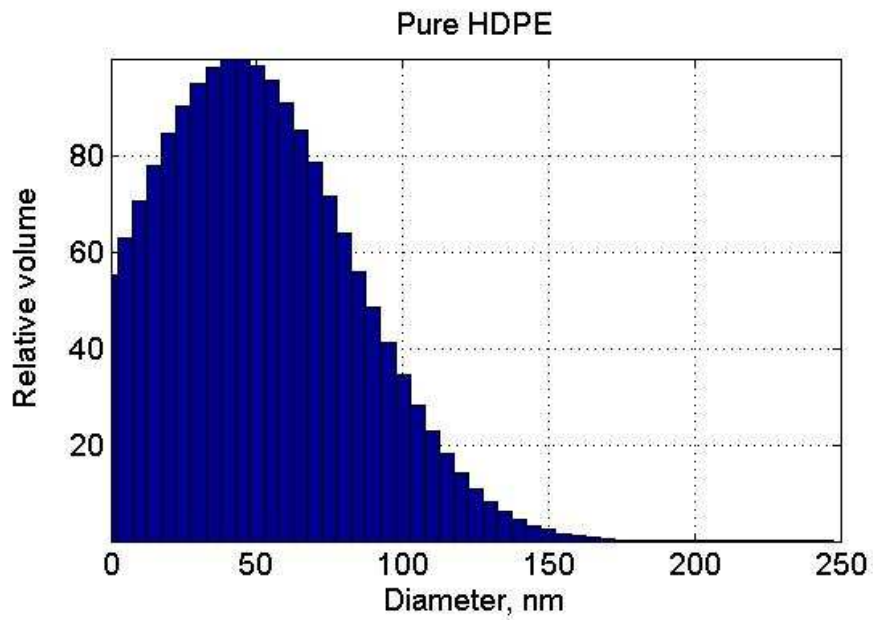
Figure 45. Idealized Gaussian distribution of wear particle diameter.

9. SUMMARY

9.1. Discussion

In the thesis, the problem of lubrication and wear of HDPE at a metal/HDPE contact was considered theoretically and experimentally.

Fully coupled fully implicit elasto-hydrodynamic problem solution approach was developed. Numerical solution algorithm allowed consideration of the problem in a wide range of physical parameters without special reference. Major parameters such as velocity, viscosity, elastic modulus were varied for theoretical calculations in the range of 0.2 mm/s to 1000 mm/s, 1-1000 cP, 1 GPa to 200 GPa correspondingly. It means that conditions varied from low velocities to very high, from low viscous liquid to high and from soft material to hard. In considered cases, calculated minimum film thicknesses varied from the order of 10 µm down to about 1 nm and solutions were obtained in maximum 40 Newton-Raphson iterations. Thus, the numerical solver was shown to be robust and to have high convergence rate.

Incorporation of surface roughness was shown to be important for the estimation of friction coefficient and for wear simulation. Addition of one asperity with height of twice as much as minimum film thickness for smooth case to the theoretical model showed increase in local friction coefficient in about order of magnitude up to 0.06, which is close to the dry friction performance. At the same time, local pressure also increased almost twice, increasing local wear rate for the same amount, according to Archard's law.

Coupled simulation of EHL theory and Archard's wear law was performed in the thesis. In this case, transient problem solutions were obtained. Based on experimental measurements for four hour long wear test, wear coefficient was found to be

about $10^{-15} \frac{m^3 N}{m}$. However, it was shown that this value changes with wear regime, encountered when increased wear time was considered.

From the measurements of surface roughness after the wear test and theoretical calculations of minimum film thickness it was concluded that the mixed lubrication regime was encountered for the considered range of parameters. In this case, dry contact between asperities occurs, which leads to increase in experimentally measured friction coefficients. However, theoretical model does not account for it, thus, making estimated friction coefficients much lower compared to experimental values. This observation also leads to the conclusion that part of the load is carried by dry contact of asperities. However, in theoretical model the load is assumed to be carried solely by liquid, which means that hydrodynamic pressures are overestimated in developed solutions. According to Archard's law, it means that wear coefficients are underestimated in this case.

The size of wear particles induced by wearing was addressed in the thesis. These debris were found to be about 100 nm in diameter and spherical in shape. Corresponding theoretical solution showed that the minimum film thickness was about 52 nm. Thus, as it was discussed above, penetration of such particle into the contact will lead to increased local friction and local pressure. According to Arhcard's wear law, increased pressure results in increased wear rate. Thus, not only surface asperities can give rise to abrasive wear mechanism, but also wear induced particles, and in this case, it will be third-body abrasive mechanism. Due to low elastic modulus of HDPE, the plastic surface is highly deformable and hence, such particles may still penetrate to the contact, even though the separation film thickness is twice smaller than the size of the debris.

Considered range of viscosities of Newtonian glycerol-water mixture lubricants was close to the range of viscosities encountered in synovial liquid in joints. Experimental measurements showed that there was a certain range of viscosities resulting in minimum wear mass loss and friction coefficient. It was also found that trends in behavior of friction coefficient were close to that of mass loss. Thus, these parameters are closely related in the system.

9.2. Recommendations for future research

Developed theoretical model offers great possibilities for further research of friction and wear simulation. From that standpoint, topics addressed in the thesis are only several items from what can be studied.

At first, transition to the 3D theoretical model is needed. In the thesis, a 2D problem was considered; however, in this case, some simplifications were necessary to be assumed, in particular, when 3D load was translated into 2D load. These simplifications introduce some error and must be excluded in future. It should be noted that developed approach can be employed for the development of such model, requiring only re-formulation of the equations in 3D.

Further, the issue of mixed lubrication model must be addressed. As it was already stressed, a mixed lubrication condition is encountered in considered range of parameters and direct contact between surfaces occurs. This regime is most likely occurs in artificial joints. Hence, it is attractive to investigate the possibility of modeling dry contact incorporated to the coupled EHL solution approach. Important issue here would be a transition from lubricated to the dry contact. From the point of view of developed in the thesis model, it is not possible to distinguish between these contacts as the EHL theory

does not contain any information on dry contact. If such theory would be developed, correct distribution of load between lubricated and dry contacts might be obtained, which would lead to correct assessment of pressures in contact and, hence, wear coefficients. Also, although it is referred to as dry or direct contact, it is not clear, whether the fluid film is completely removed from the surface or not. For example, addition of low viscosity liquid, such as water, decreases the friction coefficient significantly compared to the dry case, meaning that there might be some thin boundary film.

More attention must be paid to the influence of surface roughness on the solution. Directly measured values must be incorporated to the model and through such solutions, it may be possible to estimate parts of total friction coefficients raised by direct and lubricated contacts.

Another interesting topic for the future studies is the solution of transient problems. It is worth to consider this case, as the speeds encountered in joints vary during the walking cycle from 0 to about 0.3 m/s due to changes in velocity direction. Locations where the velocity becomes zero are important, because there increased wear rate will be encountered. From the point of view of EHL theory, steady-state solution will give a zero separation thickness for zero velocity. However, the transient solution of reciprocation motion will not due to additional dissipation term in Reynolds equation. Thus, solution of such problem will give information on the raised film thicknesses and hence, wear in points of velocity re-direction.

Another important topic to address is the non-Newtonian behavior of the synovial fluid. When the mentioned above transient problem is considered, non-Newtonian behavior of the lubricant becomes essential due to variation of viscosity with shear rates. Thus,

incorporation of this effect is necessary for the wear and friction simulation of synovial liquid.

10. BIBLIOGRAPHY

A., Saverio. *Wear of orthopaedic implants and artificial joints.* Woodhead Pub., 2012.

Ai, X. *Numerical Analysis of Elastohydrodynamically Lubricated Line and Point Contacts with Rough Surfaces By Using Semi-system and Multigrid Methods.* Evanston: Northwestern University, 1993.

Akchurin A., Xu S.,Tangpong A.,Akhatov I.,Tian-Liu. "Nanoscale Characterization of Wear Particles Produced From CNF-Reinforced HDPE Composites." *IMECE Annual Meeting.* Houston, 2012.

Archard, J.F. "Contact and Rubbing of Flat Surfaces." *Journal of Applied Physics* 24, no. 8 (1953): 981-988.

Atwood S. A., Kennedy F. E., Currier J. H., Van Citters D. W., Collier J. P. "In Vitro Study of Backside Wear Mechanisms on Mobile Knee-Bearing Components." *Journal of Tribology* 128 (2006): 275-281.

Benabdallah H., Olender D. "Finite element simulation of the wear of polyoxymethylene in pin-on-disc configuration." *Wear* 261 (2006): 1213-1224.

Cameron, A. *Basic Lubrication Theory.* Chichester: Ellis Horwood Limited, 1976.

Charnley, J. "The wear of plastics materials in the hip joint." *Plastics and rubber*, 1976: 59-63.

Cheng, N.-S. "Formula for the Viscosity of a Glycerol-Water Mixture." *Industrial and Engineering Chemistry Research* 47 (2008): 3285-3288.

Dowson D., Higginson G.R. "A Numerical Solution to the Elastohydrodynamic Problem." *Journal of Mechanical Engineering Science*, 1959: 6-15.

—. *Elasto-Hydrodynamic Lubrication. SI Edition.* Guildford: Pergamon Press Ltd., 1977.

Evans H. P., Hughes T.,G. "Evaluation of deflection in semi-infinite bodies by a differential method." *Proc Instn Mech Engns Vol 214 Part C*, 2000: 563-584.

Evans H.P., Hughes T.G. "Evaluation of Deflection in Semi-Infinite Bodies by a Differential Method." *Proc Instn Mech Engrs* 214, no. Part C (1999): 563-584.

Fisher J., Dowson D., Hamdzah H. , Lee H.L. "The effect of sliding velocity on the friction and wear of UHMWPE for use in total artificial joints." *Wear* 175 (1994): 219-225.

Floberg, L. *PhD Thesis, On Hydrodynamic Lubrication with Special Reference to Cavitaion in Bearings.* Johanneberg: Chalmers University of Technology, 1961.

Fuller, Dudley D. *Theory and Practice of Lubrication for Engineers.* New York: A Wiley-Interscience Publication, 1984.

Gao L. M., Meng Q.E.,Wang F.C.,Yang P.R.,Jin Z.M. "Comparison of numerical methods for elastohydrodynamic lubrication analysis of metal-on-metal hip implants: multi-grid versus Newton–Raphson." *Proceedings of the Institution of Mechanical Engineers, Part J: Journal of Engineering Tribology* 221 (2007): 133–140.

Goenka P, Booker J. "Spherical bearings: static and dynamic analysis." *Transactions of ASME,Journal of Lubrication Technology* 39 (1980): 103–111.

Gohar, R. *Elastohydrodynamics.* London: World Scientific Publishing Co. Pte. Ltd., 1988.

Grubin A.N., Vinogradova I.E. *Investigation of The Contact of Machine Components.* Moscow: Central Scientific Research Institute for Technology and Mechanical Engineering (TsNITMASH), 1949.

H., Okamura. "A Contribution to the Numerical Analysis of Isothermal Elasto-Hydrodynamic Lubrication." *Tribology of reciprocating engines:Tribology of Reciprocating Engines: Proceedings of the 9-th Leeds-Lyon Symposium on Tribology*, 1982: 313-320.

Hartinger, M. *CFD Modelling of Elastohydrodynamic Lubrication, PhD dissertation.* London: University of London, 2007.

Hasim Khan, Prawal Sihna, Anupam Saxena. "A Simple Algorithm for Thermo-Elasto-Hydrodynamic Lubrication Problems." *International Journal of Research and Reviews in Applied Sciences, 1:3*, 2009: 265-279.

Hu Y.Z. Wang H., Wang W.Z. ,Zhu D. "A computer model of mixed lubrication in point contacts." *Tribology International, Vol 34*, 2001: 65-73.

Hughes, T.G., Elcoate C.,D., Evans H.,P. "Coupled solution of the elastohydrodynamic line contact problem using a differential deflection method." *Proc Instn Mech Engnrs, Vol 214, Part C*, 2000: 585-598.

Ingham E., Fisher J. "The Role of Macrophages in Osteolysis of Total Joint Replacement." *Journal of Biomaterials* 26 (2005): 1271-1286.

Jagatia M., Jin Z. M. "Elastohydrodynamic lubrication analysis of metal-on-metal hip prostheses under steady state entraining motion." *Proceedings of the Institution of Mechanical Engineers, Part H: Journal of Engineering in Medicine* 215 (2001): 531–541.

Jalali-Vahid D, Jin Z M, Dowson D. "Elastohydrodynamic lubrication analysis of hip implants with ultra high molecular weight polyethylene cups under transient conditions." *Proceedings of the Institution of Mechanical Engineers, Part J: Journal of Engineering Tribology* 217 (2003): 767–777.

Johnson, K.L. *Contact mechanics.* Cambridge: Cambridge University Press, 2003.

K.C., Ludema. *Friction, Wear, Lubrication: a textbook in Tribology.* Ann Arbor: CRC Press, Inc., 1996.

Kennedy F.E., Van Citters D.W. "Lubrication and Wear of Artificial Knee Joint Materials in a Rolling/Sliding Tribotester." *Journal of Tribology* 129 (2007): 326-335.

—. *Natural and Human Joints.* in press: R. Bruce, ed, 2012.

Kima N. H., Wona D., Burris D., Holtkamp B., Gessel G. R., Swanson P., Sawyera W. G. "Finite element analysis and experiments of metal/metal wear in oscillatory contacts." *wear* 258 (2005): 1787–1793.

Kurtz S., Ong K., Lau E., Mowat F., Halpern M. "Projections of Primary and Revision Hip and Knee Arthroplasty in the United States from 2005 to 2030." *The Journal of Bone and Joint Surgery* 89 (2007): 780-785.

Liu, Q. *Friction in Mixed and Elastohydrodynamic Lubricated Contacts Including Thermal Effects.* Enschede: University of Twente, 2002.

Lugt P.M., Morales-Espejel G.E. "A Review of Elasto-Hydrodynamic Lubrication Theory." *Tribology Transactions* 54 (2011): 470-496.

Mattei L., Di Puccio F., Piccigallo B., Ciul E. "Lubrication and wea rmodelling of artificial hip joints : A review." *Tribology International*, n.d.

Meng H.C., Ludema K.C. "Wear models and predictive equations: their form and content." *Wear* 181-183 (1995): 443-457.

Mukrasa S., Kima N.H., Sawyera W. G., Jackson D.B., Bergquist L. "Numerical integration schemes and parallel computation for wear prediction using finite element method." *Wear* 266 (2009): 822-831.

Neville, A., Morina, A., Liskiewicz, T. and Yan, Y. "Synovial joint lubrication – does nature teach more effective engineering lubrication strategies?" *Proceedings of the Institution of Mechanical Engineers, Part C: Journal of Mechanical Engineering Science* 221, no. 10 (2007): 1223-1230.

Ning Ren, Dong Zhu, W.W. Chen, Q. Jane Wang. "Plasto-Elastohydrodynamic Lubrication in Point Contacts." *Journal of Tribology, Vol 132*, 2010.

Petrusevich, A. I. "Fundamental Conclusions from the Contact-Hydrodynamic Theory of Lubrication." *Izv. Akad. Nauk SSSR, vol 2*, 1951: 209.

Reynolds, O. "On the Theory of Lubrication and Its Application to Mr. Beauchamp Tower's Experiments, Including an Experimental Determination of the Viscosity of Olive Oil." *Philosophical Transactions of the Royal Society of London, vol 177*, 1886: 157-234.

Riccardo Pietrabissa, Manuela Raimondi, Elena Di Martino. "Wear of polyethylene cups in total hip arthroplasty: a parametric mathematical model." *Medical Engineeering and Physics*, 1998: 199-210.

Sargeant A., Goswami T. "Hip Implants: Paper V. Physiological Effects." *Materials and Design* 27 (2006): 287-307.

Spikes, H. A. "Sixty Years of EHL." *Lubrication Science, vol 18*, 2006: 265-291.

Szeri, Andras Z. *Fluid Film Lubrication. Theory and Design, Fluid Dynamics.* Delaware: University of Delaware, 2005.

Timoshenko S., Goodier J.N. *Theory of Elasticity.* New York: McGraw-Hill Book Company, Inc., 1951.

Venner C.H., Lubrecht A.A. *Multilevel Methods in Lubrication.* Amsterdam: Elsevier, 2000.

Venner, C.H. *Multilevel Solution of the EHL Line and Point Contact Problems, PhD Thesis.* Enschede: University of Twente, 1991.

Wang F.C., Jin Z.M. "Prediction of elastic deformation of acetabular cups and femoral heads for lubrication analysis of artificial hip joints." *Proceedings of the Institution of Mechanical Engineers, Part J: Journal of Engineering Tribology* 218 (2004): 201–209.

Wang, A. "A unified theory of wear for ultra-high molecular weight polyethylene in multi-directional sliding." *Wear* 248 (2001): 38-47.

Wannasria S., Panina S.V., Ivanova L.R., Kornienko L.A., Piriyayon S. "Increasing Wear Resistance of UHMWPE by Mechanical Activation and Chemical Modification Combined with Addition of Nanofibers." *Procedia Engineering* 1 (2009): 67-70.

Wijnant, Ysbrand Hans. *Contact Dynamics in the field of Elastohydrodynamic Lubrication, PhD dissertation.* University of Twente, 1998.

Wood W.J., Maguire R.G., Zhong W.H. "Improved Wear and Mechanical Properties of UHMWPE–Carbon Nanofiber Composites through an Optimized Paraffin-Assisted Melt-Mixing Process." *Composites* 42 (2011): 584-591.

Wu, S.R. "A Penalty Formulation and Numerical Approximation of the Reynolds-Hertz Problem." *International Journal of Engineering Science* 24, no. 6 (1986): 1001-1013.

Xu S., Tangpong A. "Review: Tribological behavior of polyethylene-based nanocomposites." *Journal of Materials Science* 47 (2012).

Zhu D., Hu Y.-Z. "Effects of Rough Surface Topography and Orientation on the Characteristics of EHD and Mixed Lubrication in Both Circular and Elliptical Contacts." *Tribology Transactions, 44:3*, 2001: 391-398.

Zhu D., Martini A.,Wang W., Hu Y., Lisowsky B., Wang Q. J. "Simulation of Sliding Wear in Mixed Lubrication." *Transactions of ASME, Vol 129*, 2007: 544-552.

11. APPENDIX

The listing of the main program code developed in Matlab is presented here.

```matlab
function num_calc()

clc;
close all;

% %%%% parameters %%%%%%%%%%%%%%%
R = 2.5*10^-3; % Radius, m
P0 = 101325; % Pa
Um = 2*pi*R/2; %%% m/s U1 = 2piR => Um = U1/2
U1 = 2*Um;
mu0 = 0.383; %%% Pa*s %%% viscosity at P0, Pa*s %% 0.383 - viscosity of
%%%% 95% glycerol-water mix at 24 C
Wl = 3; % Newtons
Wll = Wl/(0.4*R); % Newtons/m
Pc = P0; % Pa, cavitation pressure
Er = 2*1.05*10^9/(1-0.35^2); %% reduced elastic modulus, if Poisson ratio
for HDPE = 0.35, E = 1.05*10^9 Pa, Poisson ratio = 0.35
%Er = 2*200*10^9/(1-0.3^2)*1.5; %% for steel
% %%%%%%%%%%%%%%%%%%%%%%%%%%%%%%%

global alpha;
%%%%%% pressure-density-viscosity coefficients
alpha = 5.9 *10^-9; % pressure-viscosity coefficient; here for glycerol
%%%%%%%%%%%%%%%%%%%%%%%%%%%%%%%%%%%%%%%%
U1 = 2*Um %%% speed of lower surface, m/s
Ltrack = 2*pi*R; %%% track length (wear track from pin on disk), m
Ltr_d = Ltrack/R; %%% dimensionless track length
Ncycles = 1; %%% number of wear cylces %%% number of revolutions of pin

%%%% dimensionless parameters %
global A_C;
global Wld;
global Pcd;
global CE;
global gamma_h; %%% fully implicit cavitation boundary parameter

gamma_h = 10^6;
u1d = U1/Um;
A_C = R*P0/(12*mu0*Um);
Wld = Wll/(R*P0);
Pcd = (Pc - P0)/P0;
C = Pcd;
CE = -4*P0/(pi*Er);
%%%%%%%%%%%%%%%%%%%%%%%%%%%%%%%
%%%% non dimensional parameters, Dowson-Higginson
G = alpha*Er;
U = mu0*Um/(Er*R);
W = Wll/(Er*R);
%%%%%%%%%%%%%%%%%%%%%%%%%%%%%%%
%%% define number of nodes
```

```matlab
Npoints = 500; %%% in a local line (where the pressure and wear is
calculated)
%%%%%%%%%%%%%%%%%%%%%%%%%%%%%%%%%%%%%%%%%%%%%%%%%%%%%

%%%%%%% introduce global line (wear track) %%%%%%%%%%%%%%%%%%%%%%%%%%%%%%
dx_tr = 0.01;
Xtr = [0:dx_tr:Ltr_d];
Ntr = length(Xtr);
Wglobal = zeros(1,Ntr);
Wear_track = zeros(1,Ntr); %%% intorduce vector of wear (wear in each
loacation)
dt = dx_tr/u1d; %%% dimensionless time of travelling from one location on
t = 0; %% initial time variable
tmax = Ncycles*Ltr_d/u1d; %%% duration of the modelling is the total path
%%%%%%%%%%%%%%%%%%%%%%%%%%%%%% devided by speed %%%%%%%%%%%%%%%%%%%%%%%%%%%%
flag_t = 0; %%% set the intial time stop flag, 0 - continue, 1 - stop;
x_star = 0; %%% begining point (left border of the pressure build up)
%%%%%%%%%% it is going to change by x_start = x_start + u1d*dt=x_start +
%%%%%%%%%% dx_tr
%%%%%%%%%%%%%%%%%%%%%%%%%%%%%%%%%%%%%%%%%%%%%%%%%%%%%%%%%%%%%%%%%%%%%%%%%%
%%%%% declare pressure boundary values, dimensionless
Pleft = 0;
Pright = 0;
%%%%%%%%%%%%%%%%%%%%%%%%%%%%%%%%%%%%%%%%%%%%%%%%%%%%%%%%%%%%%%%%%%%%

%%%%  initial value of H0 and pressure can be found from
%%%%% analytical solution for isoviscous rigid body solution of
%%%%% Reynolds equation
global left_border;
global step_ksi;
left_border = -pi/2.0004;
step_ksi = 0.001;
%%%%%%% find ksic for a given parameters %%%%%%
[ksic fval exitflag]=
fminsearch(@find_ksic,0.5,optimset('MaxFunEvals',15000,'MaxIter',12000));
if exitflag~=1
    display('Algorithm did not converge');
end
%%%%%%%%%%%%%%%%%%%%%%%%%%%%%%%%%%%%%%%%%%%%%%%%%
%%%% calculate pressure for given parameters %%%%
[Pan xan aan xcan ksian ksican wan] = calc_p(ksic);
%%%%%%%%%%%%%%%%%%%%%%%%%%%%%%%%%%%%%%%%%%%%%%%%%
H0 = aan;
xc = xcan;
%ao = 4.9*mu0*Um*R/Wll; %%% analytical solution of the rigid case, Pc = 0
%%%%%%%%%%%%%%%%%%%%%%%%%%%%%%%%%%%%%%%%%%%%%%%%%%%%%%%%%%%%%%%%%%%%%%%%%%%%
%%
%%%%%% download an initial guess for pressure and film thickness, if
%%%%%% available
load 'matlab_W_5_true_P_new.mat'; %%% downloads X, P, H, xc, H0
x_el = X;
xc = xc*1.1;
%%%%% construct initial guess in P and H %%%%%%%%%%
left_boundary = -0.15;
right_boundary = xc;
dx = (right_boundary - left_boundary)/Npoints;
```

```matlab
X = [left_boundary:dx:right_boundary];
Pin = interp1(x_el,P,X)'; %%% interpolate downloaded solution to the
current grid
Hin = interp1(x_el,H,X)'; %%% interpolate downloaded solution to the
current grid
HT = Hin;
XT = X;
Pin(end) = P(end);
idx = find(isnan(Pin) == 1);
Pin(idx) = 0;
idx = find(isnan(Hin) == 1);
if isempty(idx)==0
    Hin(idx) = H0 + X(idx).^2/2;
end
HT = Hin; %%%% film thickness of the previous time step
XT = X;
PT = Pin;
%%%%%%%%%%%%%%%%%%%%%%%%%%%%%%%%%%%%%%%%%%
%%%% Hertz Solution of dry contact %%%%%%%%%%
bh = sqrt(8*Wll*R/(pi*Er));
tmp = 1 - (X.*R).^2/(bh^2);
idx = find(tmp<=0);
tmp(idx) = 0;
Ph = 2*Wll/(pi*bh)*sqrt(tmp);
Pmh = 2*Wll/(pi*bh);
%%%%%%%%%%%%%%%%%%%%%%%%%%%%%%%%%
%%%% roughness parameters
global a;
global xstart;
global Amp; %%%%% sin amplitude
global w_frequency;%%%% sin frequency
w_frequency = 50*4;
xstart = 0.04;
a = 0.5*10^-4;
a = 0; %%% no roughness
Ampl = 35*10^-9; %%% meters, no roughness, 0.5 - works
Amp = Ampl/R; % dimensionless
Amp = 0;
%%%%%%%%%%%%%%%%%%%%%%%%%%%
%%% wear parameters
kw_dimensions = 1.83*10^-17; %%% m^2/N, taken from the article
kw = kw_dimensions*P0; %%% dimensionless
kw= kw*1.2*128.9793;
kw = 0;
%%%%%%%%%%%%%%%%%%%%
%%%%%%% coordinates shift parameters %%%%%%%%%%%%%%%%%%%%%%%%
Lleft = 0.15; %%% initial dimensionless distance to left from tha ball
tip
%%%%%%%%%%%%%%%%%%%%%%%%%%%%%%%%%%%%%%%%%%%%%%%%%%%%%%%%%%%%%%%
%%%% service variables %%%%%%%%%%%%%%%%%
P_ALL = {};
X_ALL = {};
H_ALL = {};
H0_ALL = {};
XC_ALL = {};
l = 1; %%%
%%%%%%%%%%%%%%%%%%%%%%%%%%%%%%%%%%%%%%%%%%%
```

```matlab
%%%%%%%%%%%%%%%%%%%%%%%%%%%%%%%%%%%%%%%%%%%
N = length(X);
% %%%% calculate elastic deflection matrix nuclear
D = zeros(N,N);
for i = 1:N
        xi = (X(i) + X(i) + dx)/2;
        for j = 1:N
            D(i,j) = part_integral_elastic_line( xi, X(j), X(j) + dx);
        end
end
D = D*CE;
%%%%%%%%%%%%%%%%%%%%%%%%%%%%%%%%%%%%%%%%%%%%
Ncycles_counter = 1;
while flag_t==0
     tic
     [P H H0 X Wlocal_accumulated] = calc_pressure(Pin, Hin,PT, HT,XT,
 H0, X,D,R,dt,t,kw,u1d,Lleft,Xtr,Wglobal,alpha_dim,z,P0);
     time = toc;
     display(strcat('Solution time:',num2str(time)));
     %%%%%%%%%%%%%%%%%%%%%%%%%%%%%%%%%%%% %%%%%%%%%%%%%%%%%%%%%%%%
     %%%% calculate total wear in a local mesh %%%%%
     indexes = 1:length(P);
     w_local = wfind(P,indexes,dt,kw,u1d,Wlocal_accumulated);
     %%%%%%%%%%%%%%%%%%%%%%%%%%%%%%%%%%%%%%%%%%%%%%%
     if X(end) <= Ltr_d %%%% in case if inside of the track
         Wglobal_temp = interp1(X,w_local,Xtr)'; %%% interpolate local
pressure to a global mesh
         idx = find(isnan(Wglobal_temp) == 1);
         Wglobal_temp(idx) = 0;
         idx = Wglobal_temp~=0;
         Wglobal(idx==1) = Wglobal_temp(idx==1);
     else %%%% on the border of a periodical solution
         idx = find(X<=Ltr_d);
         Wglobal_temp = interp1(X(idx),w_local(idx),Xtr)'; %%% interpolate
local pressure to a global mesh
         idx = find(isnan(Wglobal_temp) == 1);
         Wglobal_temp(idx) = 0;
         idx = Wglobal_temp~=0;
         Wglobal(idx==1) = Wglobal_temp(idx==1);
         idx = find(X>Ltr_d);
         Wglobal_temp = interp1(X(idx)-Ltr_d,w_local(idx),Xtr)'; %%%
interpolate local pressure to a global mesh
         idx = find(isnan(Wglobal_temp) == 1);
         Wglobal_temp(idx) = 0;
         idx = Wglobal_temp~=0;
         Wglobal(idx==1) = Wglobal_temp(idx==1);
     end
     if l==1 %%% save first undisturbed film thickness (time = 0)
         Xinit = X;
         Pinit = P;
         Hinit = H;
     end
         Lleft = Lleft + u1d*dt;
         if Lleft>=Ltr_d
             Lleft = 0.15;
             Ncycles_counter = Ncycles_counter +1;
             display(strcat('Cycle number:',num2str(Ncycles_counter)));
```

```matlab
            end
            t = t + dt;
            x_star = x_star + u1d*dt;
            if t>tmax
                 flag_t = 1;
            end
            P_ALL{l,1} = P;
            H_ALL{l,1} = H;
            X_ALL{l,1} = X;
            H0_ALL{l,1} = H0;
            XC_ALL{l,1} = xc;

            if mod(l,24)==0
                plot(Xtr,Wglobal,'r');
                hold on;
            end

        l=l+1
        HT = H;
        PT = P;
        X = XT; %%%% make X as at the begining ('local');
        Hin = H;
        Pin = P;

        %%%%%%% save all variables %%%%%%%%%%%%%%%%
        save(strcat('all',num2str(dx),'.mat'));
        %%%%%%%%%%%%%%%%%%%%%%%%%%%%%%%%%%%%%%%%%%

end
 %%%% equation for ksic (for numerical solution) %%%%%%%%%%%%%%
function goal_val = find_ksic(ksic)
global Pcd;
global A_C;
global Wld;
f1 = load_equation(ksic);
f2 = pc_equation(ksic);
goal_val = abs(2*Pcd/(sqrt(A_C)*Wld^(3/2)) - f2/(f1)^(3/2));
%%%%%%%%%%%%%%%%%%%%%%%%%%%%%%%%%%%%%%%%%%%%%%%%%%%%%%%%%%%%%%%%%
%%%% first equation of the system (from load balance)%
function W = load_equation(ksic)
c1 = -1/cos(ksic)^2;
W = 0.5*(1+3/4*c1)*(1+(ksic+pi/2)*tan(ksic)) + 1/8;
%%%%%%%%%%%%%%%%%%%%%%%%%%%%%%%%%%%%%%%%%%%%%%%%%%%%%%%%%%

%%%% second equation of the system (from Reynolds equation) %%
function P = pc_equation(ksic)
c1 = -1/cos(ksic)^2;
P = 1/8*sin(2*ksic)*(1+3/2*c1)+1/2*(1+3/4*c1)*(ksic+pi/2);
%%%%%%%%%%%%%%%%%%%%%%%%%%%%%%%%%%%%%%%%%%%%%%%%%%%%%%%%%%%%%%%
%%%% Pressure function %%%%%%%%%%%%%%%%%%%%%%%%%%%%%%%%%%%%%%%
function [P x a xc ksi ksic w] = calc_p(ksic)
global A_C;
global Wld;
global Pcd;
global left_border;
global step_ksi;
```

```matlab
f1 = load_equation(ksic);
a = 2*f1/(A_C*Wld);


c1 = -1/cos(ksic)^2;
k = 3*pi/16*c1+pi/4;


ksi = left_border:step_ksi:ksic;


P = sqrt(2*a)/(a^2*A_C)*(1/4.*sin(2.*ksi) + ksi./2 +
c1.*(1/32.*sin(4.*ksi) + 1/4.*sin(2.*ksi) + 3.*ksi./8) + k);


x = sqrt(2*a).*tan(ksi);


xc = sqrt(2*a)*tan(ksic);


w = 2*load_equation(ksic)/(a*A_C);


%%%%%%%%%%%%%%%%%%%%%%%%%%%%%%%%%%%%%%%%%%%%%%%%%%%%%%%%%%%%%%%%%%
function [P H H0 X Wlocal_accumulated] = calc_pressure(Pin, Hin,PT,
HT,XT, H0, X,D,R,dt,t,kw,u1d,Lleft,Xtr,Wglobal,alpha_dim,z,P0);


global Wld;
global gamma_h;
global Amp;
global w_frequency; %%%% frequency


N = length(X);
X = X + Lleft;
Wlocal_accumulated = zeros(1,N)';
%%% interpolate global accumulated wear to a new local X coordinates
%%%%%%
    if X(end) <= Xtr(end) %%%% in case if inside of the track
        Wlocal_accumulated = interp1(Xtr,Wglobal,X)';
        idx = isnan(Wlocal_accumulated) == 1;
        Wlocal_accumulated(idx) = 0;
    else %%%% on the border of a periodical solution
        idx = find(X<=Xtr(end));
        Wlocal_accumulated(idx) = interp1(Xtr,Wglobal,X(idx))';
        idx = isnan(Wlocal_accumulated) == 1;
        Wlocal_accumulated(idx) = 0;
        idx = find(X>Xtr(end));
        Wlocal_accumulated(idx) = interp1(Xtr,Wglobal,X(idx)-Xtr(end))';
        idx = isnan(Wlocal_accumulated) == 1;
        Wlocal_accumulated(idx) = 0;
    end
%%% assign initial guess on pressure and h
    P = Pin;
    H = Hin ;
%%%%%%%%%%%%%%%%%%%%%%%%%%%%%%%%%%%%%%%%%%%%%%%%%%%%%
V = zeros(2*(N-2)+2,1);
idxp = 1:2:(2*(N-2));
idxh = 2:2:(2*(N-2));
V(idxp) = P(2:N-1);
V(idxh) = H(2:N-1);
```

```matlab
Nt = length(V);
V(Nt-1) = H(end);
V(end) = H0;
Vt = V; %% vestor for the previous iteration

flag = 0;
k = 1;
w_all = 0.01;
mu_w = 1 - w_all; %%% aetkins parameter
mu_wp = mu_w;
w_all_p = w_all;

NormL2_all_p = [];
NormLinf_all_p = [];
NormL2_all_h = [];
NormLinf_all_h = [];
NormL2_all_h0 = [];
NormLinf_all_h0 = [];

while flag == 0
    Jacobian =
find_jacobian(P,X,H,R,D,H0,dt,kw,u1d,Lleft,alpha_dim,z,P0,Amp,w_frequency
);
    F =
find_f_vector(P,X,H,PT,HT,R,D,H0,Wld,dt,t,kw,u1d,Lleft,Wlocal_accumulated
,alpha_dim,z,P0);
    if k >2
        Lkhp = NormL2_h;
    end
    if k == 20
        w_all = 0.1;
    elseif k==30
        w_all = 1;
    end

    if mod(k,50)==0;
        display('Stop');
    end
    tic
    setup.type = 'nofill';
    [A1 A2] = luinc(sparse(Jacobian),setup);
    tol = 1e-12;
    maxit = 15;
      [Vn flag_gmres relres iter] = gmres(Jacobian,Jacobian*V -
F,10,tol,maxit,A1,A2);
        if relres>10^-9
            display('Warning: GMRES did not converge!');
            relres
            iter
     end
    time=toc;
    display(strcat('Solution time:',num2str(time)));

    Epsilon = sum(abs(Vn-V)./abs(V));
    Pn = Vn(idxp);
    Pt = V(idxp);
```

```matlab
    idx = find(Pt~=0);
    NormL2_p = sum(((Pn(idx) -
Pt(idx))./abs(Pt(idx))).^2);%./NormL2_all_p(end);
    NormL2_h = sum(((Vn(idxh)-
V(idxh))./V(idxh)).^2);%./NormL2_all_h(end);
    NormL2_h0 = sum(((Vn(end)-V(end))./V(end)).^2);%./NormL2_all_h0(end);

    NormLinf_p = abs(max((Vn(idxp)-
V(idxp))./V(idxp)));%./NormLinf_all_p(end);
    NormLinf_h = abs(max((Vn(idxh)-
V(idxh))./V(idxh)));%./NormLinf_all_h(end);
    NormLinf_h0 = abs(max((Vn(end)-
V(end)))./V(end));%./NormLinf_all_h0(end);

    NormL2_all_p = [NormL2_all_p NormL2_p];
    NormL2_all_h = [NormL2_all_h NormL2_h];
    NormL2_all_h0 = [NormL2_all_h0 NormL2_h0];

    NormLinf_all_p = [NormLinf_all_p NormLinf_p];
    NormLinf_all_h = [NormLinf_all_h NormLinf_h];
    NormLinf_all_h0 = [NormLinf_all_h0 NormLinf_h0];
     V(idxp) = w_all.*Vn(idxp) + (1-w_all).*V(idxp);  %% P
     V(idxh) = w_all.*Vn(idxh) + (1-w_all).*V(idxh); %% H
     V(Nt-1) = w_all.*Vn(Nt-1) + (1-w_all).*V(Nt-1);  %% Hn
     V(end) = w_all*Vn(end) + (1-w_all)*V(end); %% H0;
    dP = (P(end) - P(N-1))/abs(X(1)-X(2));
    if NormL2_p < 0.0000099532 && abs(dP)<1500;
        flag = 1;
    end
    residual = sum(abs(Jacobian*F));
    Vn = V;
    P(2:N-1) = Vn(idxp);
    P(1) = 0;
    P(N) = 0;
    H(2:N-1) = Vn(idxh);
    H(N) = Vn(Nt-1);
    H0 = Vn(end);
    display(strcat('Newtons iteration:',num2str(k)));
    k = k + 1;
    if k>1000
        flag = 1;
    end
    display(strcat('L2 norm p:',num2str(NormL2_p)));
    display(strcat('L2 norm h:',num2str(NormL2_h)));
    display(strcat('L2 norm h0:',num2str(NormL2_h0)));
    display(strcat('dP:',num2str((P(end) - P(N-1))/abs(X(1)-X(2)))));
    display(strcat('F:',num2str(sum(F.^2))));
end
```